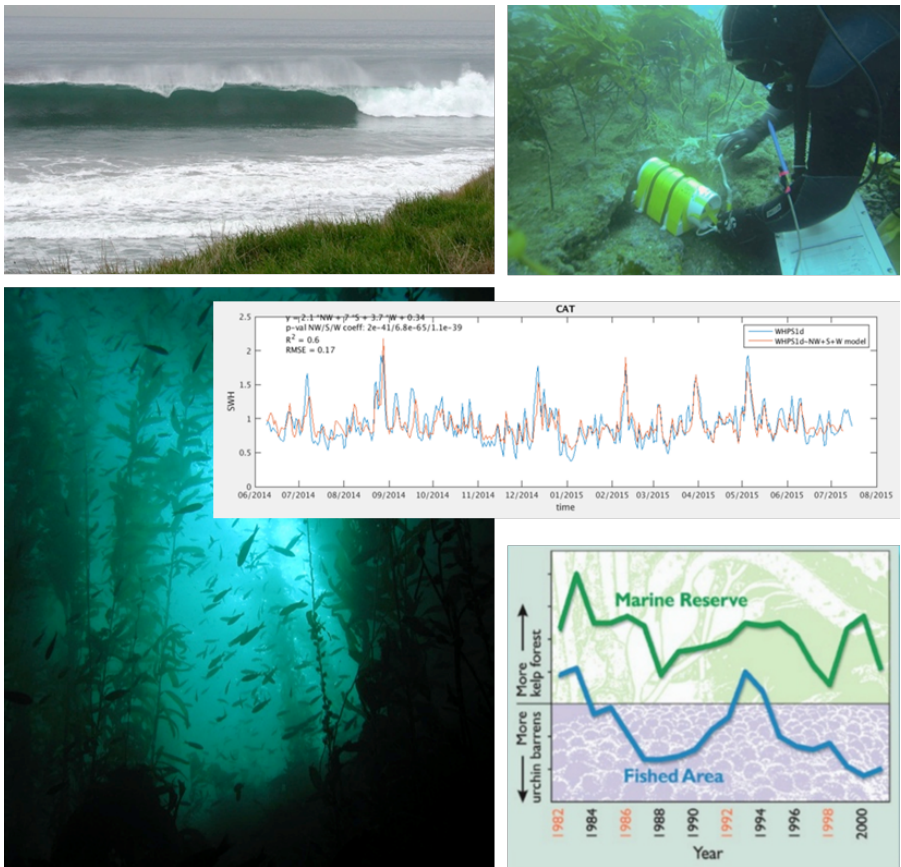


The Response of Kelp Forest Organisms to Spatial and Temporal Variation in Wave Energy in the California Channel Islands



The Response of Kelp Forest Organisms to Spatial and Temporal Variation in Wave Energy in the California Channel Islands

December 2019

Authors:

Lafferty, K.D.¹, Rassweiler, A.², Gotschalk, C.C.², Morton, D.N.², Bell, T.W.², Henderikx Freitas, F.²,
Kushner, D.J.³, Sprague, J.³, Johnson, C.³ and Washburn, L.²

¹ Western Ecological Research Center, U.S. Geological Survey

² Marine Science Institute, University of California Santa Barbara

³ Channel Islands National Park

Prepared under an Intra-Agency Study Plan

By

U.S. Department of the Interior

U.S. Geological Survey

Western Ecological Research Center

In cooperation with:

Marine Science Institute

University of California

Santa Barbara, CA 93106

U.S. Department of the Interior

Channel Islands National Park

1901 Spinnaker Drive

Ventura, CA 93001

US Department of the Interior
Bureau of Ocean Energy Management
Pacific OCS Region



DISCLAIMER

This study was developed by the U.S. Geological Survey in consultation with the Bureau of Ocean Energy Management (BOEM) through an Intra-Agency Study Plan, and conducted in part using a subcontract to the University of California Santa Barbara (UCSB). This report has been technically reviewed by BOEM, and it has been approved for publication. This product has been peer reviewed and approved for publication consistent with USGS Fundamental Science Practices (<http://pubs.usgs.gov/circ/1367/>). Any use of trade, firm, or product names is for descriptive purposes only and does not imply endorsement by the U.S. Government.

REPORT AVAILABILITY

To download a PDF file of this report, go to the US Department of the Interior, Bureau of Ocean Energy Management [Data and Information Systems webpage](http://www.boem.gov/Environmental-Studies-EnvData/) (<http://www.boem.gov/Environmental-Studies-EnvData/>), click on the link for the Environmental Studies Program Information System (ESPIS), and search on 2019-064.

CITATION

Lafferty, K.D., Rassweiler, A., Gotschalk, C.C., Morton, D.N., Bell, T.W., Henderikx, F., Kushner, D.J., Sprague, J., Johnson, C., and Washburn, L. 2019. The response of kelp forest organisms to spatial and temporal variation in wave energy in the California Channel Islands. Camarillo (CA): US Department of the Interior, Bureau of Ocean Energy Management. OCS Study BOEM 2019-064. 38 p.

ABOUT THE COVER

Cover photos by K.D. Lafferty, USGS.

ACKNOWLEDGMENTS

Donna Schroeder (BOEM) helped initiate the study and provided constructive advice. David Salazar (UCSB) provided essential assistance with calibration and transport. Mark Torchin, John McLaughlin, Lauren Dykman, Donna Schroeder and Susan Zaleski (BOEM) assisted with deployment and retrieval. Mark Torchin provided an internal peer review. Corey Olfe and James Behrens advised on using CDIP hindcasts to align sensor data. James Behrens reviewed and commented on a draft report. Stanley Reifel helped with sensor engineering. David Salazar and Eduardo Romero constructed the sensors. David Salazar calibrated most of the sensors. Donna Schroeder took the photograph in Figure 5.2.

Contents

List of Figures.....	ii
List of Tables.....	ii
List of Abbreviations and Acronyms.....	iii
1 Introduction.....	1
1.1 Background and Objectives	1
1.2 Description.....	2
1.3 Significant Results	2
2 Executive Summary	4
2.1 Information Needed	4
2.2 Research Summary.....	4
2.3 Conclusions	5
3 Wave Height Varies Across the Southern California Bight	6
3.1 Introduction.....	6
3.2 Methods.....	6
3.3 Results and Discussion	7
4 An Inexpensive and Accurate Sensor for Measuring in-situ Wave Height and Period.....	10
4.1 Introduction.....	10
4.2 Methods.....	12
4.3 Results and Discussion	14
5 Sensor Deployment Around the Channel Islands	16
5.1 Introduction.....	16
5.2 Methods.....	17
5.3 Results and Discussion	19
6 Using Sensor Data to Assess CDIP Hindcast Accuracy.....	21
6.1 Introduction.....	21
6.2 Methods.....	21
6.3 Results and Discussion	21
7 Using Sensor Data to Correct Hindcast Bias	24
7.1 Introduction.....	24
7.2 Methods.....	24
7.3 Results and Discussion	24
8 Building a Corrected Hindcast Database for Wave Energy at Kelp Forest Monitoring Sites.....	28
8.1 Introduction.....	28
8.2 Methods.....	28
8.3 Results and Discussion	28
9 Estimating Biological Responses to Wave Energy	29
9.1 Introduction.....	29
9.2 Methods.....	29
9.3 Results and Discussion	30
10 Predicting the Consequences of Wave Energy Absorption from Marine Renewable Energy Facilities on Nearshore Ecosystems.....	35
10.1 Introduction.....	35
10.2 Methods.....	35
10.3 Results and Discussion	35
11 References	37

List of Figures

Figure 2.1.	Summary of the steps that should be taken when determining the potential implications of extracting wave energy.	4
Figure 3.1.	Hourly swell heights (as quartiles) from Harvest Buoy from 2014-2017.	7
Figure 3.2.	Hourly swell direction (as quartiles) from Harvest Buoy from 2014-2017.	8
Figure 3.3.	Spatial variation in wave height across in summer and winter seasons.	9
Figure 4.1.	Photos of the final WHPS wave measuring pressure sensor.	11
Figure 4.2.	Example of laboratory calibration of WHPS.	12
Figure 4.3.	a) Bottom pressure $p(t)$, b) Significant wave height H_s , and c) peak wave period T_p from two WHPSs and a SeaBird 26+ wave tide recorder.	14
Figure 4.4.	Comparing correspondence with time interval (left raw, right daily).	15
Figure 5.1.	Thirty-two kelp forest monitoring locations where we deployed pressure sensors.	16
Figure 5.2.	Pressure sensor within a housing, weighted down by lead bricks.	18
Figure 6.1.	Plot of observed vs modeled daily wave height across 32 sites, with best-fit lines per site. ...	22
Figure 6.2.	Plot of observed (Daily Sensor Period) vs modeled (Daily Model Period) daily wave period across 32 sites, with best-fit lines per site.	23
Figure 9.1.	Modeled species density (note the logged axis) plotted against orbital bottom velocity for 20 species with significant responses to wave energy.	33
Figure 10.1.	Modeled species densities before (blue) and after (red) a 15% reduction in wave height at an exposed site.	36

List of Tables

Table 5.1.	Site names, location and depth, including post-processing validation.	17
Table 5.2.	Sensor deployments, by site, including post-processing validation.	19
Table 7.1.	List of total (1.18 + site) per-site bias (standard error), total correction coefficient (inverse of total bias), and R^2 for a simple no-slope model for wave height.	26
Table 7.2.	List of bias (standard error), correction coefficients (inverse of bias), and R^2 for a simple no-slope model for wave period.	27
Table 9.1.	Significant standardized regression coefficients indicating density associations by species (algae in green, invertebrates in red and fishes in blue text), to various potential drivers.	31

List of Abbreviations and Acronyms

BOEM	Bureau of Ocean Energy Management
CDIP	Coastal Data Information Program
DOI	US Department of the Interior
ESP	Environmental Studies Program
ESPIS	Environmental Studies Program Information System
GPS	Global Positioning System
MREI	Marine Renewable Energy Installation
NPS	National Park Service
UCSB	University of California, Santa Barbara
USGS	U.S. Geological Survey
WEC	Wave Energy Conversion
WERC	Western Ecological Research Center
WHPS	Wave-Height Pressure Sensors

1 Introduction

1.1 Background and Objectives

The mission of the U.S. Geological Survey (USGS) is to provide reliable scientific information to describe and understand the Earth, minimize loss of life and property from natural disasters, manage water, biological, energy, and mineral resources, and enhance and protect the quality of life. To this end, the USGS collects, monitors, analyzes, and provides scientific understanding about natural resource conditions, issues, and problems. The USGS Western Ecological Research Center (WERC) provides its clients and partners with the research, scientific understanding, and technology needed to support sound management of Pacific ecosystems.

The mission of the Bureau of Ocean Energy Management (BOEM) is to manage development of energy and mineral resources found on the outer continental shelf in an environmentally and economically responsible way. To this end, BOEM seeks to assess and understand how the bureau's decision-making impacts the environment, and how those impacts can be avoided or minimized.

Because ocean renewable energy projects are new to the west coast of the US, there is considerable uncertainty about the types of impacts that they might have. Others have considered impacts to viewsheds, or navigation risks, barriers to animal migrations, seafloor disturbances at moorings, or disturbance from transmission cables and servicing (Nelson et al. 2008). Less well understood is how wave energy extraction devices, by removing energy from waves, might affect nearshore marine communities (Shields et al. 2011), and this has been identified as a topic of concern in the Pacific Region (Boehlert et al. 2013). Theoretical models predict that wave energy conversion (WEC) devices will suppress wave height in their wake, with the magnitude varying according to a range of site-specific factors including water depth and configuration of the WEC array (EPRI 2004, Nelson et al. 2008). A reasonable maximum estimate of wave height reduction at the shoreline appears to be 15% (Nelson et al. 2008), and it is this value we use in our analysis to assist BOEM in predicting potential impacts from leasing activities associated with marine renewable energy. Most studies have considered the extent that wave height reduction would have on currents and sediment transport, but few have asked specifically how organisms might respond.

There is considerable evidence that wave energy can affect intertidal marine communities where the bulk of wave energy is expended (Jensen and Denny 2015). For instance, in their classic text on intertidal biology, Between Pacific Tides, Ricketts and Calvin (1939) divide rocky-associated species according to the wave environment (Bays and Estuaries, Protected Outer Coast, Open Coast). Far less is known about subtidal species which, by virtue of living at depth, might be relatively unaffected by wave energy. One exception to this is the giant kelp, *Macrocystis pyrifera*. Giant kelp is an important habitat-forming species and food source. Individuals attach to rocks with a holdfast, and are sufficiently adapted to exposed coasts that waves pass through thick kelp beds with little energy loss (Elwany et al. 1995). Kelp does better in moderate wave energy than in still water, perhaps due to the delivery of nutrients, or reduced competition from species less adapted to higher energy environments (Hepburn et al. 2007; Bell et al. 2015). Regardless, under extreme conditions, kelp can be ripped from the bottom by large waves (Reed et al. 2011). Other algae (England et al. 2008), and fishes (Munks et al. 2015) also respond to wave energy in different parts of the world. Because so many marine species are associated with giant kelp in the study region, there is potential for indirect effects of wave energy extraction on species that themselves are not directly affected by wave energy. Regardless, with little actual information, the effects of wave energy extraction are hard to predict.

Some of the classic work on how waves affect marine species has been mechanistic and experimental. Such experiments show that many marine species have adaptations like firm attachment structures or flexible bodies to help deal with the strong forces that wave energy can impose (Gaylord et al. 2001).

The ultimate purpose of this study was to develop a statistical model that predicts the potential effects of wave energy absorption from marine renewable energy facilities on nearshore ecosystems such as kelp forests or shallow (< 30 m) rocky reefs. The need for this information is to predict which siting alternatives of proposed wave energy facilities may generate detectable changes in nearshore ecosystems, especially kelp forests. BOEM will use results from this study for impact assessments contained within documents required by the National Environmental Policy Act, and also in essential fish habitat coordination and consultation requirements established by the 1996 reauthorization of the Magnuson-Stevens Fishery Conservation and Management Act.

1.2 Description

The report has 10 sections that describe the various steps needed to reach the final goal. The first section evaluates the spatial and temporal variation in wave height for the study system in the broader context of the Southern California Bight. This helps identify two wave seasons as well as the distribution of exposed and protected sites in the region. We then describe the design of a new, low-cost pressure sensor that measures height and period. Most of the project was spent deploying, retrieving and processing sensors at 32 sites around the Channel Islands where long-term kelp forest monitoring occurs. We then compared hourly data from the sensors with hourly hindcasts from the Coastal Data Information Program (CDIP). This made it possible to generate simple statistical corrections to CDIP hindcasts to help improve their accuracy. With this correction, we generated hourly hindcasts for all of our sites back to the year 2000. Then, to understand how wave energy might drive species dynamics, we created another data set, this time with annual wave energy measures, for 88 sites with biological data. We analyzed these data to find associations between abiotic factors and species density in time and space. We also asked how species densities would change in response to a 15% reduction in wave height at a high-energy site suitable for energy extraction.

Author contributions. Lafferty designed and oversaw the project, deployed and retrieved sensors, analyzed data, and wrote reports, Rassweiler designed sensor housing and deployment protocol, guided the integrated data set, and managed the cooperative agreement to UCSB, Gotschalk processed sensor data, estimated hindcasts, and aligned hindcasts with sensor data, Morton tracked and organized sensor logs, deployed and retrieved sensors, and coordinated wave energy databases. Bell scraped historical CDIP data to estimate wave climate and spatial distribution in the bight, Henderikx explored associations between sensor data and buoy data, Kushner and Sprague deployed and retrieved sensors. Johnson designed the wave sensor, and Washburn worked with Gotschalk on the processing and analysis of the sensor data. All authors contributed to this final report.

1.3 Significant Results

The prevailing swell in Southern California Bight is from the northwest. However, the May-September summer season is characterized by an absence of large swells, and the presence of swells from the south. Pt. Conception creates a substantial wave shadow that blocks northern swells, whereas the Channel Islands block swells from the west and the south. There are three focal areas for large winter swells: west San Miguel Island, west San Nicolas island, Tanner Bank and Cortez Bank. The custom-built sensors were improved, with the final version being reliable and deployable for over 9 months. These sensors were far less expensive than commercially available units and could be useful for other applications

where replicated information on non-directional wave energy is needed. The biggest expense and effort in our project was putting sensors out at remote field sites. Our sensors indicated that the CDIP model underestimated wave height around the islands, similarly as it is known to underestimate wave height along the mainland coast in the Santa Barbara Channel. CDIP periods were not biased, but were less precise, probably due to the bimodal periods that often occur when wind swell mixes with groundswell. A statistical model provided a simple way to correct CDIP hindcasts, though a few sites required more complicated corrections. By fitting a statistical model to the bias corrections, we were able to generalize corrections to any site in the Channel Islands region based on swell window and location. After controlling for site-specific effects, and other drivers like sea surface temperature, chlorophyll, substrate, depth, and turbidity, we found that wave energy (expressed as bottom orbital velocity in m/s) had a significant effect on several species. But for most taxa (36/56), density was unrelated to waves. Even for those species with a statistical relationship between density and orbital velocity, we found that a 15% reduction in wave height would not have a detectable effect on the density of any species. As a result, a reduction in wave height due to renewable energy projects is unlikely to result in substantial changes to a wide range of nearshore subtidal species in southern California.

2 Executive Summary

2.1 Information Needed

As the permitting agency for ocean renewable energy in federal waters, BOEM has need for guidance on the potential impacts of a 10-15% wave height reduction. Unfortunately little is known about relationships between wave energy and nearshore marine species. Shields et al. (2011) outlines the process needed to obtain the information required to evaluate the ecological consequences of extracting wave energy (Figure 2.1). We applied the left-hand side of this approach (green boxes) to the northern Channel Islands, because long-term monitoring throughout this regions makes it uniquely suited to meet the first and key requirement for this process (top left box Figure 2.1: identify species and habitats and their distribution). To estimate associations between wave energy and species abundances requires annual wave energy information matched to these sites (bottom left box, Figure 2.1). Understanding the influence of hydrodynamics on identified species and habitats is challenging in our region (Hegermiller et al. 2017), and therefore required collecting wave energy data. We then used statistical models to apply our models to a hypothetical Marine Renewable Energy Installation (MREI) that was placed at an exposed location and reduced wave height by 15%.

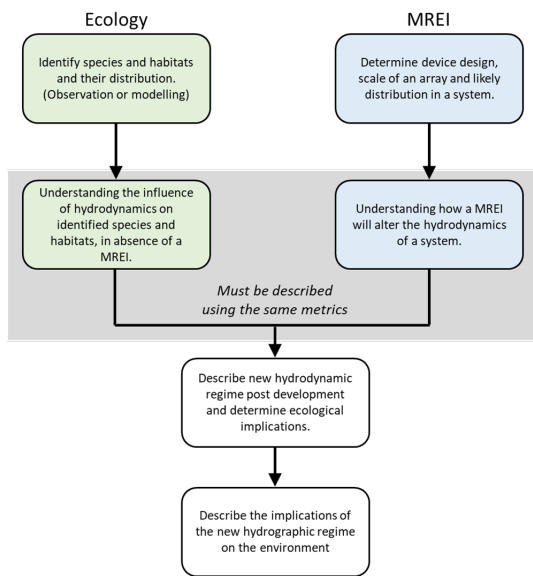


Figure 2.1. Summary of the steps that should be taken when determining the potential implications of extracting wave energy (adapted from Shields et al. 2011). MREI stands for Marine Renewable Energy Installation.

2.2 Research Summary

This report describes the spatial and temporal variation in wave height for the study system in the broader context of the Southern California Bight. A new, low-cost pressure sensor was engineered for measuring wave height and period. These sensors were placed for several months at 32 sites around the Channel Islands where long-term kelp forest monitoring occurs. Matching sensor data with CDIP wave hindcasts made it possible to correct the CDIP model hindcast to make it applicable to nearshore sites in this region. With these corrections, annual wave energy was estimated for 88 sites where long term biotic monitoring had been conducted in the study region. These data were analyzed to assess the extent that wave energy

affects species abundances and, in particular, how a reduction in wave height would affect various species.

2.3 Conclusions

Across all species, only 12% of the variation in abundance in time and space was explainable by the factors in our study. Temperature explained the most variation, followed by wave orbital velocity, island/mainland, chlorophyll, diffuse attenuation, and fishing intensity. Density sensitivity to orbital velocity varied across taxa and was often non-linear. Consistent with past results (Bell et al. 2015), kelp biomass peaked at intermediate orbital velocity. For most taxa (36/56), density was unrelated to wave orbital velocity. Twenty species were statistically associated with wave energy, often in complex ways. Four species (*Apostichopus parvimensis*, *Caulolatilus princeps*, *Cymatogaster aggregata*, and *Halichoeres semicinctus*) had negative relationships with wave energy, whereas four species (*Sebastes mystinus*, *S. serranoides*, *Embiotica lateralis*, *S. miniatus*) had positive associations with wave energy. The remaining twelve species had concave (U-shaped) relationships with wave energy. At this point we do not have a hypothesis for what would create such a pattern, but it could be an indirect response to a parameter, like kelp biomass, that has a concave relationship with wave energy. Because the relationship with wave energy was often non-linear, it is difficult to predict the directional effect of wave energy extraction on species abundances.

We modeled density responses to a 15% reduction in wave height, focusing at high wave energy sites, which would be locations where wave-power would be most likely considered. Such a reduction never altered density at the $P < 0.05$ threshold. This suggests that although some species do respond to changes in bottom orbital velocity within the ranges seen in our study system, a 15% reduction in wave height at a high wave energy site was too subtle for the models to detect a change in any species density. Although no modeled changes were statistically significant, some patterns in the data are worth speculating about. If there was to be an effect of reducing wave energy at high-energy sites, these results suggest up to 14 of the 56 species could decline slightly as a response, whereas some species might respond positively. In particular, reduced wave energy might allow two wave-averse fish species to persist where they could not before. Effects in deeper water should be even more subtle (and effects in shallow water greater) than we estimate. These results help reduce uncertainty about the impacts of wave energy extraction and, therefore may inform the streamlining of permitting processes for renewable energy projects near kelp forest communities.

3 Wave Height Varies Across the Southern California Bight

3.1 Introduction

To understand how wave energy affects biological resources in the Santa Barbara Channel, it is first useful to describe how it varies. The Santa Barbara Channel is relatively protected, but the wave climate varies from season to season, with southerly swell predominating in the summer months and northwest swell directions in the winter months. This complexity affects the potential locations for when and where wave extraction can occur within the region. The complex geography of the region also leads to considerable variation in wave exposure across space.

Here, we sought to describe the wave climate of the region in terms of its seasonality and spatial variation. Directional wave information is derived from buoy motions, the power transfer functions and phase responses associated with the buoy, mooring, and measurement systems. The dependence between these signals is difficult to determine at low energy levels and at both short and long wave periods where the wave signal being measured is weak and potential for added signal contamination increases. Signal processing produces wave-height spectral data to estimate the significant heights and periods across a directional spectrum. Focusing on the energy from the wave-height spectrum, dominant period, and significant wave height measured by a sensor makes it easier to understand seasonal patterns in wave energy.

To get spatial information from the temporal wave spectra, the Coastal Data Information Program (CDIP; cdip.ucsd.edu) uses a network of deep water directional buoy measurements to initialize a linear wave propagation model (O'Reilly et al. 2016). The computationally fast model takes wave height, period and directional spectral information from buoys and propagates this information through a model of the Southern California Bight, where it estimates nearshore wave energy (heights and periods) and low-order directional spectra moments (direction) for nearshore significant surface waves along the coast. Although CDIP models hourly nearshore wave height as a function of swell direction, amplitude and period in the study region, there has not been a simple summary of wave climate for these data.

3.2 Methods

The CDIP wave hindcast model is based on data from buoys. The most informative buoy for seasonal information in our study region is the Harvest Buoy (CDIP / USACE / CA DBW buoy 071). We downloaded hourly height and direction data from this buoy for 2014-2017. We then binned the averages by month and inspected their confidence limits. Sharp breaks between adjacent months in height and direction helped us categorize wave seasons.

At the time of our study, historical information from CDIP was limited to archived hourly graphical model outputs from the CDIP nowcast wave models. Bell et al. (2015) developed an algorithm to access these hourly images from the archive and convert the images into a database. For the period from June 1998 to November 2011, coordinates were spatially registered in the X-Y plane, and then the color for each pixel was interpreted as an integer representing hourly significant wave height in meters according to the CDIP scale. With this database, it is possible to generate average values for any particular time interval and location. Due to the seasonal differences in wave energy, the most useful summary for our purpose was winter versus summer. We wished to further define the wave seasons for later statistical analyses. To do so, we analyzed the Harvest Buoy wave spectra for modality over time.

3.3 Results and Discussion

Mean significant wave height for the Southern California Bight differed during the winter (October – April) and summer (May – September) wave seasons. In this region swell direction varies by season, with northwest swells being present all-year round, but strongest in the winter and south swells being relatively rare outside the summer (Figure 3.1). These different swell directions could have different effects on sites with different exposures, and they group well into a summer season May-September and a winter season October-April (as indicated by the box in Figures 3.2 and 3.3). Hereafter, when analyzing wave data, we apply different models for summer and winter when appropriate.

Compressing thousands of CDIP hourly wave height outputs also shows that wave heights and directions differ throughout the Southern California Bight between summer and winter. Four areas stand out as having unusually high winter wave exposure as indicated by the yellow patches. From top to bottom in Figure 3.3, these are the west end of San Miguel Island, the west end of San Nicolas Island, Tanner Bank, and Cortez Bank. This map and the site-location map of Figure 5.1 also showed that our in-situ measurements covered the full range of wave climate in the southern California bight (e.g., from highly exposed sites on the west ends of San Miguel and San Nicolas Island, to highly protected sites on Anacapa Island). Pt. Conception creates a major wind and wave shadow for the region. And the Channel Islands generate substantial wave shadows for the mainland below Pt. Conception. As such, the results in this report, though focused on the Santa Barbara Channel are relevant to the Southern California Bight in general. We note that since the advent of CDIP’s hind cast algorithm, there are now direct ways to generate more in-depth wave histories for this region (as we have done in the subsequent sections of this report).

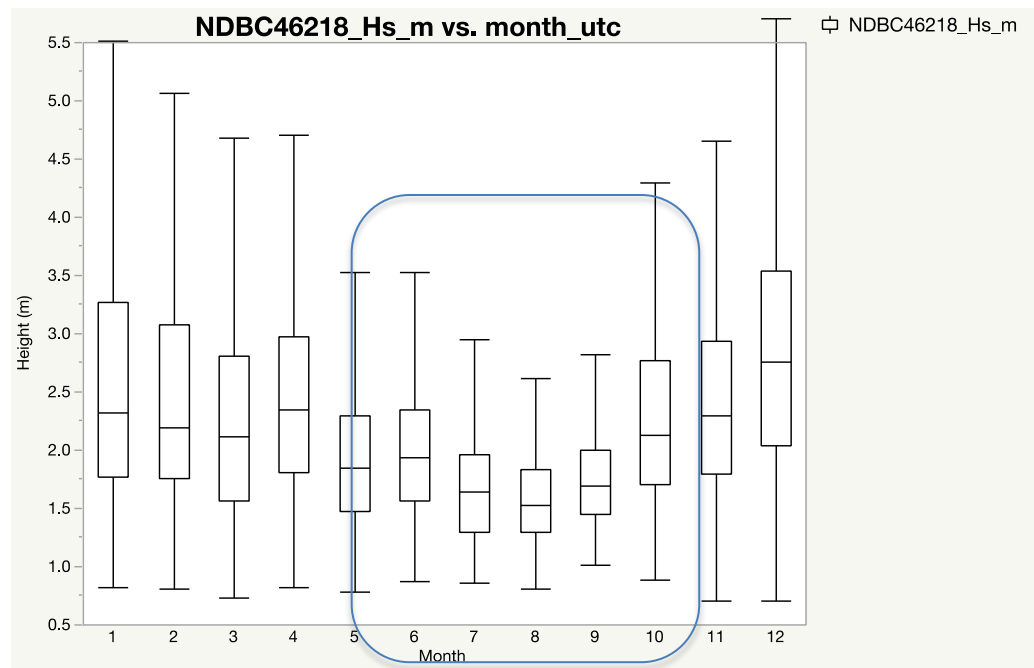


Figure 3.1. Hourly swell heights (as quartiles) from Harvest Buoy from 2014-2017. Boxed area is the proposed summer wave season.

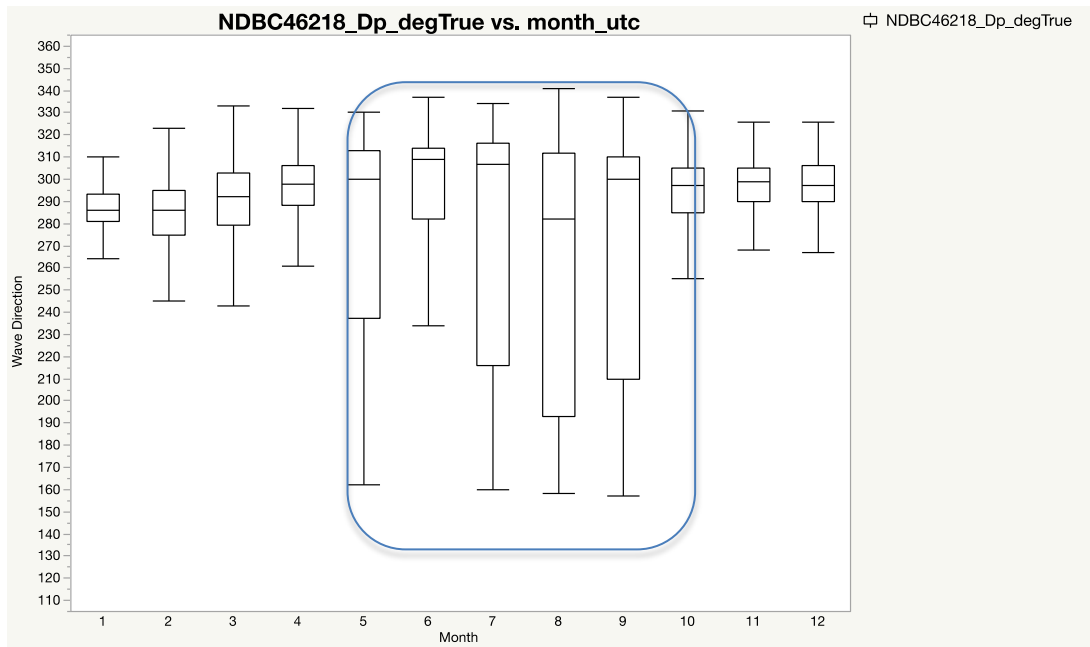


Figure 3.2. Hourly swell direction (as quartiles) from Harvest Buoy from 2014-2017. Boxed area is the proposed summer wave season.

Mean Significant Wave Height

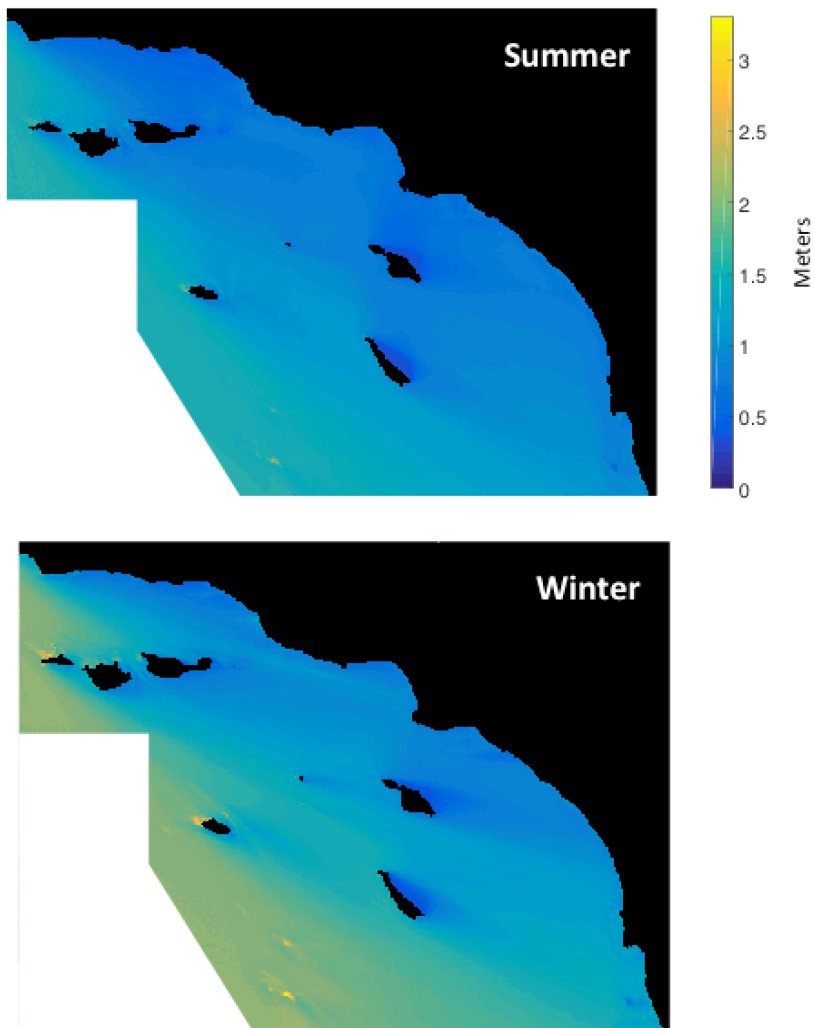


Figure 3.3. Spatial variation in wave height across in summer and winter seasons.

4 An Inexpensive and Accurate Sensor for Measuring in-situ Wave Height and Period

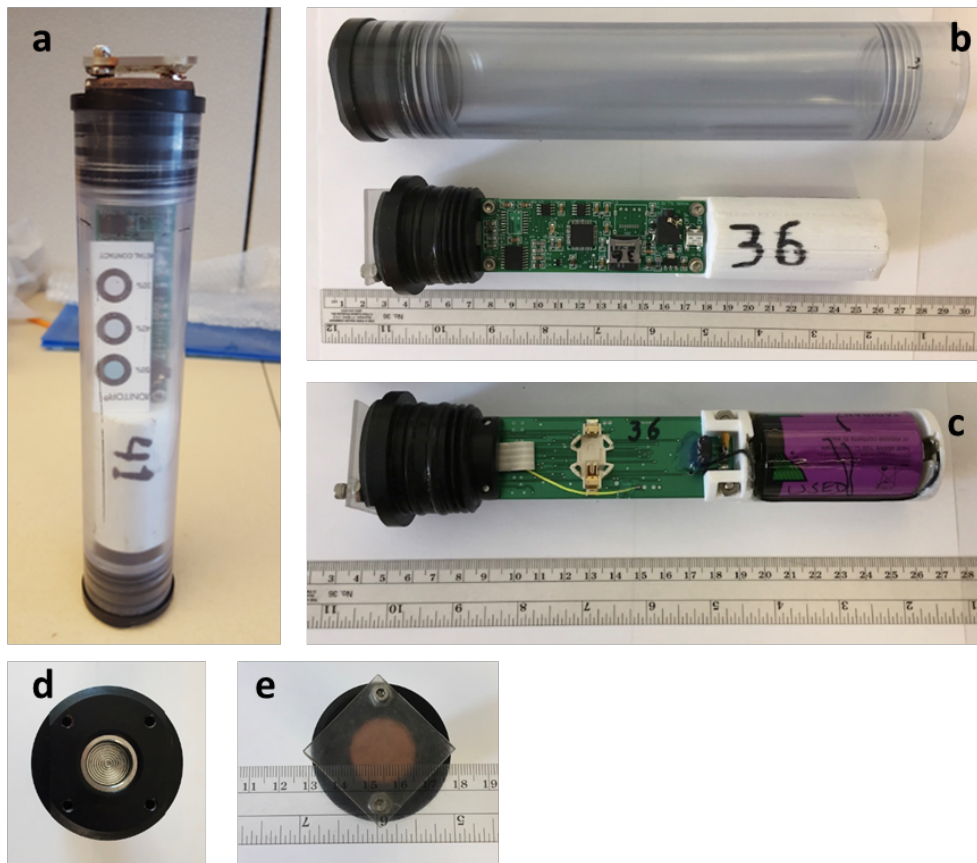
4.1 Introduction

Although Figure 3.1 is instructive, the CDIP wave models are coarse in their predictions and are not able to resolve the smaller spatial scales and shallower depths where species interact and kelp forests, which are known to be sensitive to waves, occur. Their ability is limited in indicating wave energy at different depths. Although they have been validated (and shown to be reasonably accurate) with wave sensors along the mainland coast, their accuracy around the Channel Islands has long been in doubt (O'Reilly et al. 2016, Hegermiller et al. 2017). Furthermore, although wave climates for the state of California have been modeled, estimates are lacking for the Channel Islands (Erikson et al. 2014). The physics of refracting, reflecting, and breaking waves leads to attenuation of wave forces and turbulence with depth. To extrapolate wave model predictions to forces acting on specific subtidal sites in marine communities, one must measure wave energy in the field at different depths and compare this to model predictions. Doing this at sites where ecological data have been collected for marine communities would make it possible to do several new types of analyses about how wave energy (or a change in wave energy) affects near-shore marine communities. Unfortunately, existing real-time wave energy sensors are expensive and, therefore, it would not be cost effective to deploy dozens in the field.

To achieve our goals required improvements to an existing, inexpensive, and accurate wave sensor to measure wave statistics such as significant wave height (here defined as the mean of the largest one-third of the waves recorded during 17-minute intervals) and period of surface gravity waves in water depths of about 20 m and shallower. A main design goal was to record time series of bottom pressure at sufficiently high frequencies to observe the sea level variations due to waves at the various sites. Other pressure sensors used for determining wave statistics, such as the SeaBird Electronics 26+ wave and tide recorder (hereafter SBE 26+; Sea-Bird Electronics, Inc., Bellevue, WA), measure bottom pressure at 4 Hz. This was the sampling frequency chosen for the sensor used in the project.

Several versions of the wave-height pressure sensors (WHPS) were used in the project. The versions evolved based on experience deploying the instruments in a variety of coastal ocean environments. The earliest design was powered by 4 alkaline D-cells mounted in a clear plastic tube along with the electronics board and pressure transducer. Later designs were powered by single lithium-ion D-cells with higher-energy density storage. These were enclosed in a smaller diameter tube. Other design changes were based on the availability of 3-D printing. The most recent WHPS versions used 3-D printing for the support of the electronics board and battery holder. Figure 4.1 shows a recent version of the WHPS that was used extensively in the project. All versions of the WHPS were successfully deployed in coastal waters of the Santa Barbara Channel and the Northern Channel Islands.

In contrast to other wave-measuring pressure sensors such as the SBE 26+ which record burst samples of bottom pressure, the WHPS records continuously at a sampling frequency of $f_s = 4$ Hz. Although this creates larger data files, it has the advantage of recording uniformly sampled time series. This allows considerable flexibility in post processing. Data were recorded on 2 Gbyte SD cards and deployments at remote islands lasted up to 1 year, although typical deployments were 3-6 months long.



- a) Assembled pressure sensor ready for deployment.
- b) Upper part of photo shows acrylic pressure case and end cap. Lower part of photo shows circuit board and battery holder.
- c) Reverse side of circuit board. White fixture to the left of “36” is the holder for a clock battery. Main battery is at the right side of the circuit board.
- d) End view of pressure sensor. Silver circular area is housing and diaphragm of Honeywell pressure transducer. For deployment, this is covered with copper powder and silicone grease as shown in panel e).
- e) End view of pressure sensor. Brown circle is mixture of copper powder and silicone grease, which reduces bio-fouling on exposed transducer surface. The clear plastic square protects the sensor and helps retain the silicone grease and copper powder.

Figure 4.1. Photos of the final WHPS wave measuring pressure sensor.

The pressure transducer is temperature compensated to improve performance in environments with variable temperature. During field deployments temperature is typically measured concurrently by other instruments so temperature effects can be evaluated if necessary. For example, using data from side-by-side deployments of WHPS and SBE 26+ no consistent pressure variations due to temperature changes have been detectable. To evaluate temperature sensitivity, WHPS data were sampled over times when the SBE 26+ measured a constant pressure. Anomalies in the WHPS pressure time series during times when pressure was constant were compared with available temperature time series. These comparisons did not

reveal significant correlations between temperature and pressure anomalies in the WHPS time series. This suggests that temperature effects on the WHPS time series were small.

Early versions of the WHPS used a Honeywell 19C050PA4K (Honeywell International, Inc., Charlotte, NC) pressure transducer with a threaded port that was mounted over the diaphragm and strain gauges that respond to pressure changes. This configuration proved difficult to maintain due to corrosion around the diaphragm. Based on this experience, this transducer was replaced with a similar version, Honeywell 19C050PA1K, that did not have the threaded port. Instead, the diaphragm was open, which made inspection and cleaning much easier. Figure 4.1d shows the diaphragm in the end cap of the pressure sensor. To prevent settlement of organisms on the diaphragm, the circular cavity around the diaphragm was filled with a mixture of silicone grease mixed with copper powder (Figure 4.1e). A clear-plastic protective cover was fitted just above the cavity to prevent the silicone and copper mixture from being flushed out due to water movement (Figure 4.1e). This modification proved successful. Typically the silicone and copper mixture remained in place following deployments of several months.

4.2 Methods

WHPSs were calibrated prior to each deployment. During the calibration procedure, the WHPS being calibrated was mounted on a fixture and the pressure transducer was exposed to compressed air. The air pressure was separately measured by another pressure sensor. Air pressure was increased and then decreased stepwise over a range that included the pressures corresponding to the deployment depth. In all cases the response of the pressure sensor was linear with no measurable hysteresis such as shown in Figure 4.2.

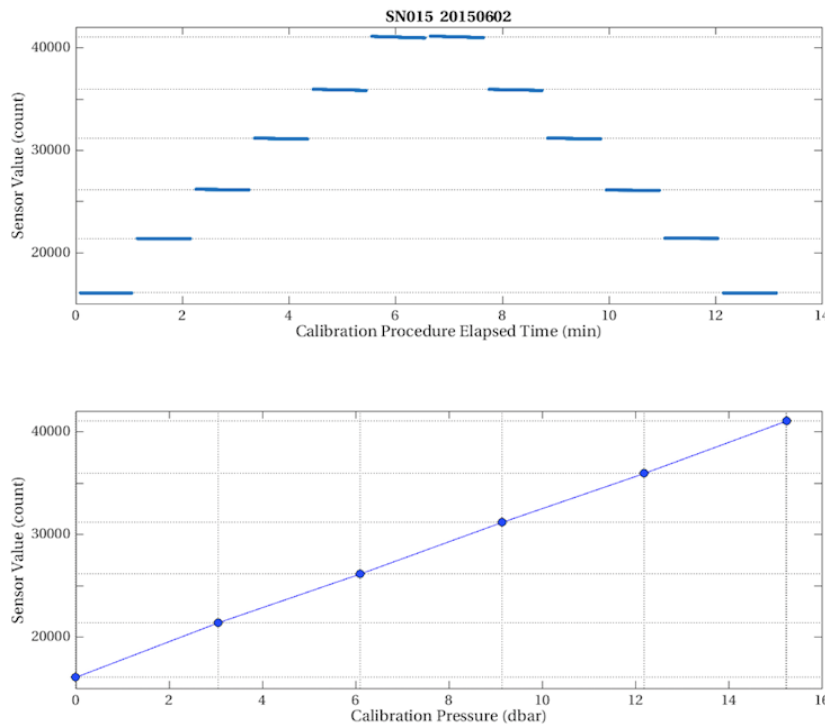


Figure 4.2. Example of laboratory calibration of WHPS. a) Time series of digital sensor counts from pressure sensor during calibration procedure. b) Digital sensor count versus pressure in dbar. Pressure of 1 dbar corresponds to depth of about 1 m.

Pressure fluctuations were converted to sea-level variations using results from the linear theory of surface gravity waves and standard methods. A fast Fourier transform algorithm (FFT) converted bottom pressure $p(t)$ from the time domain to the frequency domain $Y(f)$. Frequency f was converted to period in seconds (s) as $T = 1/f$. Then wavelength L corresponding to each frequency was computed using the dispersion relation,

$$\omega^2 = gk \tanh(kd) \quad (1)$$

where \tanh is the hyperbolic tangent, $\omega = 2\pi f = 2\pi/T$ is the radian frequency, g is the acceleration of gravity (9.81 m s^{-2}), $k = 2\pi/L$ is the wavenumber, and d is the water depth. Fourier coefficients $Y(f)$ were corrected for attenuation of pressure with depth as,

$$Y_p(f) = Y(f)/[\cosh(ks)/\cosh(kd)] \quad (2)$$

where \cosh is the hyperbolic cosine and s is the sensor height above the seafloor ($s = 0.05 \text{ m}$). An inverse FFT algorithm converted $Y_p(f)$ to sea surface height variations in the time domain $\eta(t)$. The minimum period for transforming $Y_p(f)$ to $\eta(t)$ was $T_{\min} = 4 \text{ s}$. This was done to avoid applying very large attenuation factors for waves with periods less than T_{\min} . Wave signals from periods less than T_{\min} were near or below the sensor noise level.

Significant wave height H_s and wave period T_p were estimated from autospectra of $\eta(t)$. These spectra were computed from data segments of length $M=8192$ using a transform length of $m = 4096$ samples. A Gaussian spectral window was applied and FFT estimates were overlapped by 75%. The transform length m allowed resolution of variations in $\eta(t)$ with periods ranging from $T_{\min} = 4 \text{ s}$ to $T_{\max} = m/f_s = 1024 \text{ s} \approx 17 \text{ min}$. T_p was estimated as the frequency corresponding to the peak of the autospectrum. H_s was estimated as,

$$H_s = 4 (\sigma^2)^{1/2} \quad (3)$$

where σ^2 is the variance of $\eta(t)$; σ^2 was estimated in the time domain from each data segment of length M and, as a check, by integrating the autospectra. These estimates of σ^2 typically agreed to within $\sim 20\%$.

Estimates of $\eta(t)$, H_s , and T_p , from two WHPSs and a SBE 26+ wave tide recorder are compared in Figure 4.3 from a ~ 9 -week deployment on an oceanographic mooring at Mohawk Reef (34.393°N , 119.730°W) in the Santa Barbara Channel near Santa Barbara, CA, USA. The mooring is maintained by the Santa Barbara Channel Long Term Ecological Research project. The mean bottom pressure at the site was about 10.2 dbar corresponding to a water depth of about 10.2 m. Mixed semidiurnal tidal variations are evident along with the spring-neap tidal cycle (Figure 4.3a).

H_s from both WHPSs were significantly correlated with H_s from the SBE 26+ ($r^2 = 0.94, 0.92$, for sn071 and sn072, respectively; large N) as may be seen in Figure 4.3b. Correlations were lower for T_p ($r^2 > 0.41, 0.42$, for sn071 and sn072, respectively) likely due to the greater ‘‘quantization’’ of T_p values from the SBE 26+ compared with the WHPSs. This may be seen in Figure 4.3c where T_p values from the SBE 26+ tend to align in separate horizontal rows, particularly for longer periods. This is due to differences in data processing: FFT lengths can be made longer for the WHPS data because the data are continuously sampled. In contrast, the SBE 26+ collects data in separate bursts due to memory limitations so transform

lengths are typically shorter which causes separate T_p values to be more widely spaced. Another difference between the T_p records of the WHPSs and the SBE 26+ in Figure 4.3c is the minimum value of T_p : For the WHPSs it was set to 4 s and for the SBE 26+ it was set to 5 s. Although the WHPS sensed consistently larger wave heights than the SBE 26+, we did not interpret this as WHPS overestimating wave height, for the following reasons: 1) The SBE 26+ did not have a recent factory calibration whereas the WHPS were regularly calibrated, 2) short burst sampling could cause the SBE26+ to miss some of the highest, less frequent waves that the continuous records from the WHPS's would capture. Even though we suspect that the WHPS is more accurate than the SBE 26+, overall Figure 4.3 shows good agreement between H_s and T_p obtained from the WHPSs and the SBE 26+. The data processing procedure used to produce Figure 4.3c was the same as used to process data for this study.

4.3 Results and Discussion

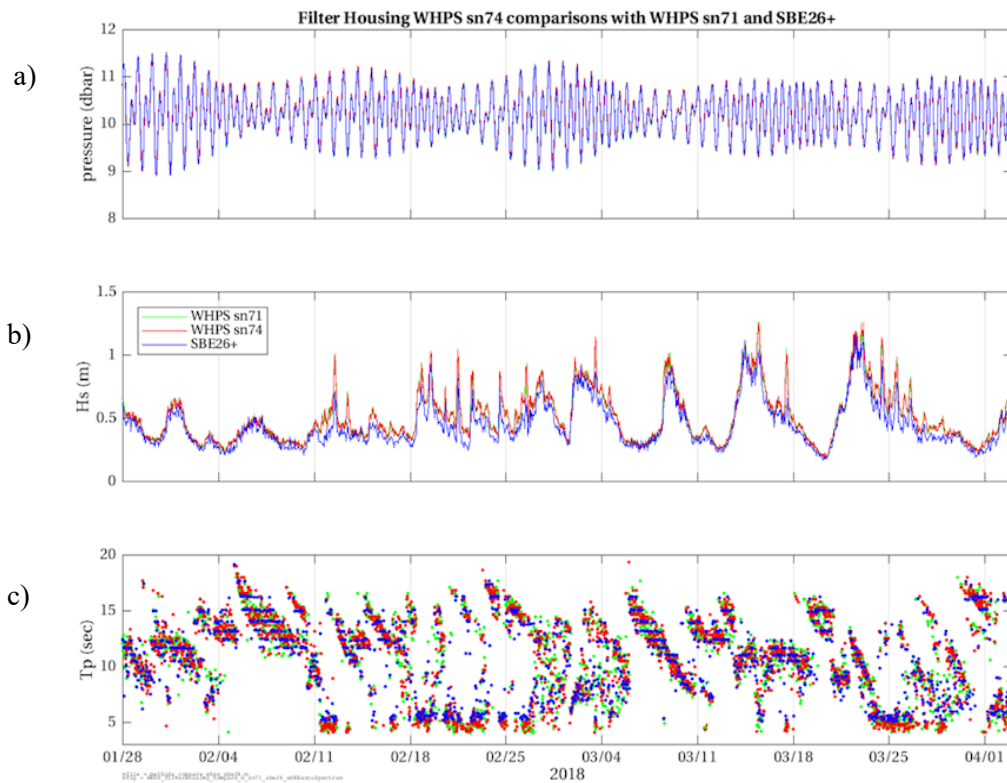


Figure 4.3. a) Bottom pressure $p(t)$, b) Significant wave height H_s , and c) peak wave period T_p from two WHPSs and a SeaBird 26+ wave tide recorder. Panel b) shows the legend.

Distances between a buoy and a site can result in time lags between a sensor observation and a wave model prediction. As can be seen in Figure 4.4, the longer the time interval, the closer the correspondence between sensor observations and model predictions (as discussed below, this is also true for correspondence between two sensors at the same site). For this reason, assessment of sensor fit to model fit is perhaps best done at daily time intervals. In addition to accounting for time lags, daily intervals, as averages, reduce the variance around the model and the sensor information. Sub-daily variance might be important for understanding the probability distribution of wave events. Specifically, using daily averages will exclude the largest and smallest wave events from the record. So, even though fits are best assessed at daily intervals, we generated data at hourly intervals (buoy data are at 30 minute intervals).

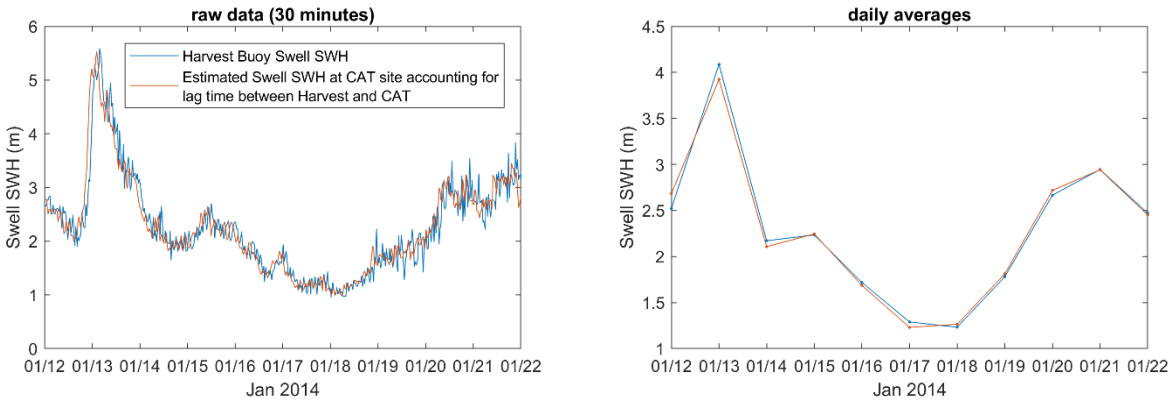


Figure 4.4. Comparing correspondence with time interval (left raw, right daily).

5 Sensor Deployment around the Channel Islands

5.1 Introduction

Our goal was to obtain in situ height and period data for both wave seasons at each long term monitoring site at each of the National Park Service (NPS) Kelp Forest Monitoring sites, and later several of the USGS Kelp Forest Monitoring sites at San Nicolas Island (Figure 5.1 and Table 5.1).



Figure 5.1. Thirty-two kelp forest monitoring locations where we deployed pressure sensors (basemap from Google fusion tables).

Table 5.1. Site names, location and depth, including post-processing validation.

Site code	Site Name	Island Name	Longitude	Latitude	Depth (m)
APX	Arch Point	Santa Barbara	-119.0275833	33.48753333	9.45
ARX	Admiral's Reef	Anacapa	-119.43407	34.00773	14.33
CAT	Cat Canyon	Santa Barbara	-119.0391667	33.46441667	7.62
CCX	Cathedral Cove	Anacapa	-119.37628	34.01546	5.49
CPX	Cluster Point	Santa Rosa	-120.18769	33.92284	10.36
CSA	Chickasaw	Santa Rosa	-120.1361333	33.9005333	10.06
CVP	Cavern Point	Santa Cruz	-119.56634	34.05454	12.50
DTN	Daytona Beach	San Nicolas	-119.44412	33.21687	10.36
EDH	East Dutch Hbr.	San Nicolas	-119.48407	33.21598	12.19
EFC	East Fish Camp	Anacapa	-119.37628	34.0042	10.97
FHX	Fry's Harbor	Santa Cruz	-119.75515	34.05635	13.11
GCX	Graveyard Cyn	Santa Barbara	-119.0268167	33.47306667	12.19
GIX	Gull Island South	Santa Cruz	-119.82754	33.94993	16.46
HRX	Hare Rock	San Miguel	-120.3566	34.06438333	7.62
JLN	Johnson's Lee N.	Santa Rosa	-120.10288	33.90179	9.14
JLS	Johnson's Lee S.	Santa Rosa	-120.10081	33.89791	16.46
KHX	Keyhole	Anacapa	-119.43146	34.01628	8.84
LCX	Landing Cove	Anacapa	-119.3611333	34.0170333	4.88
LHX	Lighthouse	Anacapa	-119.35859	34.01448	7.62
MMX	Miracle Mile	San Miguel	-120.3951333	34.0237	10.67
NFX	NavFac	San Nicolas	-119.48555	33.27351	11.28
PBX	Pelican Bay	Santa Cruz	-119.70325	34.034933	8.23
PRF	Pedro Reef	Santa Cruz	-119.525	34.03799	9.14
RRX	Rodes Reef	Santa Rosa	-120.1074	34.0328333	16.15
SAX	Scorpion Anch.	Santa Cruz	-119.551	34.04776	7.01
SER	Southeast Reef	Santa Barbara	-119.0312667	33.46293333	9.14
SES	SE Sea Lion	Santa Barbara	-119.0277833	33.46611667	12.19
SPX	South Point	Santa Rosa	-120.1195	33.8923333	11.58
WAX	Webster's Arch	Santa Barbara	-119.0622	33.47985	13.72
WEX	West End	San Nicolas	-119.57367	33.24762	10.06
WLX	Wyckoff Ledge	San Miguel	-120.3874667	34.02236667	14.02
YBK	Yellow Banks	Santa Cruz	-119.5630667	33.98983333	14.94

5.2 Methods

Divers from UCSB, USGS and NPS began to deploy WHPS sensors in December 2013. After battery installation and calibration the sensor hardware was sealed with desiccant packs and a humidity indicator, and placed in a protective polyvinyl chloride housing with approximate dimensions of 11-inch long and 4-inch diameter, bolted to a 26-lb block of lead weight (Figure 5.1) and wrapped in yellow tape to reduce fouling and increase underwater visibility.

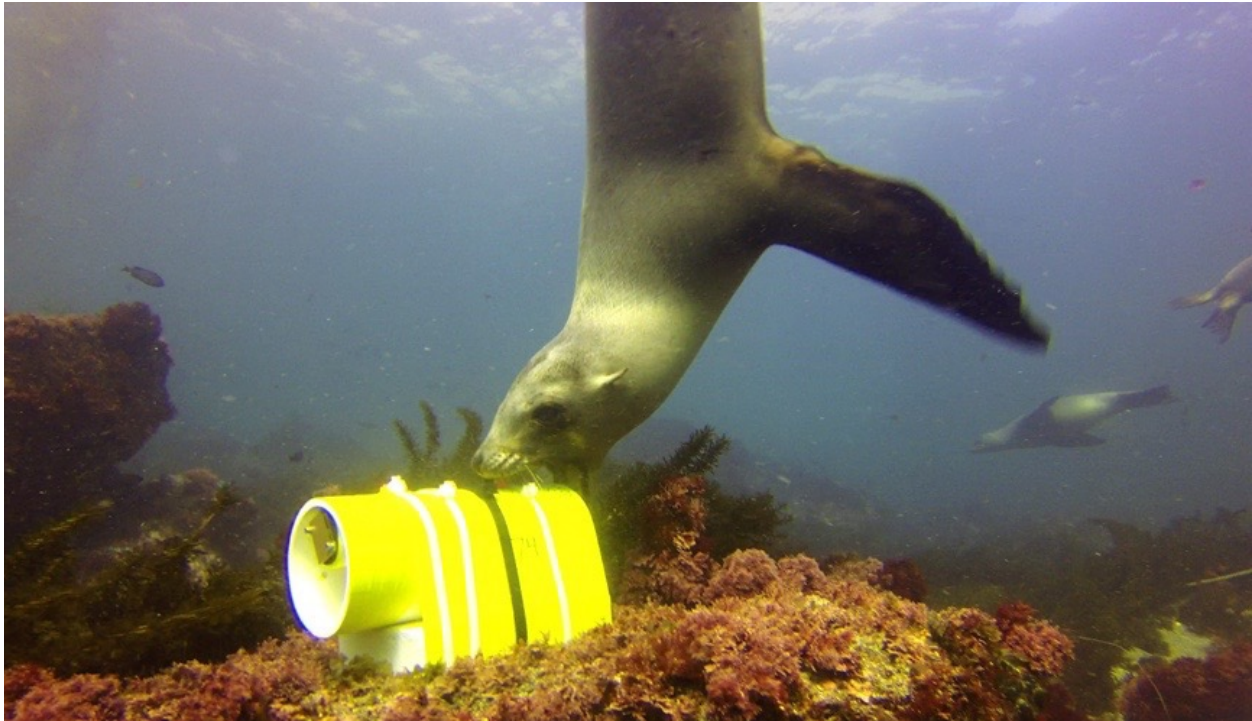


Figure 5.2. Pressure sensor within a housing, weighted down by lead bricks.

To deploy a sensor, the boat captain anchored at one end of a monitoring transect based on GPS coordinates. The sensor was connected to a lift bag, and both were attached by a clip to a tether which was lowered slightly into the water and then tied off to a cleat. Data collected by the sensor is independent of orientation. In the water, divers filled the lift bag, unclipped it, and descended the boat's anchor line. At the anchor, the sensor was staged on the bottom until the permanent transect line (marked by lead line and fixed bolts) was found. The sensor was moved to the end of the transect line and positioned in a suitable deployment position. As a result of this process, wave data come from within 10 m of areas (and at the same depths) where long term ecological monitoring is being collected, and thus directly measures the wave climate to which those communities are exposed.

Sensors were deployed for several months until being exchanged for a new sensor. Deployed sensors were often fouled and would have been difficult to find if not for their placement along the permanent transect. Sensors were retrieved by placing the housing and attached weight in a dive bag and then attaching and inflating a lift bag for a controlled ascent to the surface. On the surface, fouling organisms were cleared from the housing and the units were stored for transport.

Back at UCSB, sensors were removed from their housings, and their memory cards were removed and downloaded. WHPS pressure data in counts were downloaded from the SD cards and MATLAB was used to apply a valid calibration to each sensor, converting counts to pressure in dbar. Raw pressure time series were examined to identify and remove out of water pre- and post-deployment sections of the data record. Mean water depth was estimated by calculating the average pressure and assuming 1 dbar = 1 m.

5.3 Results and Discussion

Obstacles to successful sensor deployment included weather, which made it difficult to reach the sites further from land, failing to relocate and retrieve sensors on two occasions (likely buried or removed), failed batteries, unreliable or suspect measurements, or other sensor failures. We inspected suspicious patterns in the time series or potential drift related to battery drain. Suspect data were excluded from the analyses (Table 5.2). Problems and failures declined appreciably with experience and as the newest sensor model came into use with its better battery life. After 41 months, we retrieved the final sensor in May 2017 (Table 5.2). All hourly height and period sensor data are compiled and available online at Washburn et al. (2018). CDIP has concluded that these data would be valuable in an effort to tune their wave model to improve its reliability in the Channel Islands more generally (James Behrens pers. comm.).

Table 5.2. Sensor deployments, by site, including post-processing validation.

Site_code	Deployment	Start time	End time	Validation
FHX	1	12/12/13	02/13/14	Suspect
APX	1	06/11/14	07/13/14	Suspect
EFC	1	05/30/14	09/04/14	Good
FHX	1	03/19/14	09/24/14	Good
LHX	1	05/29/14	11/06/14	Suspect
ARX	1	05/28/14	11/25/14	Good
CCX	1	05/30/14	11/25/14	Good
JLS	1	07/18/14	12/01/14	Suspect
CSA	1	07/29/14	12/01/14	Good
CVP	1	12/12/13	12/04/14	Good
JLN	1	07/30/14	12/08/14	Suspect
SPX	1	07/31/14	12/08/14	Suspect
SAX	1	08/26/14	01/03/15	Good
LCX	1	09/29/14	01/28/15	Good
HRX	1	08/13/14	02/07/15	Good
PRF	1	08/25/14	02/08/15	Suspect
MMX	1	11/05/14	02/10/15	Good
EFC	2	11/25/14	03/11/15	Good
KHX	1	05/28/14	03/29/15	Good
LHX	1	11/25/14	04/06/15	Good
CSA	2	01/22/15	05/17/15	Good
RRX	1	08/12/14	05/19/15	Good
CPX	1	07/15/14	06/10/15	Good
JLS	1	12/19/14	06/10/15	Good
GIX	1	03/19/14	06/22/15	Good
YBK	1	03/19/14	06/22/15	Good
PRF	1	02/24/15	06/25/15	Good
APX	1	01/28/15	07/04/15	Good
CCX	2	06/29/15	07/10/15	Good
CAT	1	06/10/14	07/15/15	Good
SES	1	01/28/15	07/15/15	Good

Site_code	Deployment	Start time	End time	Validation
GCX	1	01/29/15	07/15/15	Good
WAX	1	01/29/15	07/15/15	Good
CVP	2	02/24/15	07/20/15	Good
PBX	1	08/15/14	07/31/15	Suspect
SAX	2	02/24/15	08/01/15	Good
LCX	2	06/26/15	11/21/15	Good
LHX	2	06/24/15	12/18/15	Good
PRF	2	08/14/15	03/17/16	Good
JLN	1	08/13/15	04/17/16	Good
WLX	2	09/15/15	05/09/16	Good
SER	1	01/28/15	05/26/16	Good
GCX	2	10/14/15	05/27/16	Good
SAX	3	08/14/15	05/31/16	Good
CVP	3	10/02/15	06/23/16	Good
SPX	2	08/27/15	06/27/16	Good
MMX	2	08/26/15	07/01/16	Good
WAX	2	10/13/15	07/10/16	Good
CPX	2	11/13/15	07/24/16	Good
SES	2	06/08/16	08/07/16	Good
DTN	1	10/20/15	09/13/16	Good
NFX	1	11/22/15	09/25/16	Good
WEX	1	10/22/15	09/26/16	Good
EDH	1	10/22/15	09/27/16	Good
CCX	3	06/23/16	09/27/16	Good
WLX	1	10/01/14	10/17/16	Good
PBX	1	08/28/15	12/01/16	Good
PRF	3	08/23/16	12/01/16	Good
SAX	4	08/26/16	12/01/16	Good
HRX	2	06/10/15	12/21/16	Good
MMX	3	08/11/16	01/31/17	Good
SPX	1	01/22/15	02/19/17	Good
CSA	3	11/13/15	03/14/17	Good
JLS	2	11/13/15	03/14/17	Good
SPX	3	07/13/16	03/14/17	Good
JLN	2	07/14/16	03/14/17	Good
LCX	3	12/18/15	05/01/17	Good
ARX	2	11/15/16	05/01/17	Good
SER	2	11/30/16	05/11/17	Good
SES	3	08/17/16	05/25/17	Good

6 Using Sensor Data to Assess CDIP Hindcast Accuracy

6.1 Introduction

Originally our intent was to match sensor data with Waverider[®] buoy data in order to produce wave hindcasts for each site. However, during our project CDIP developed a regional hindcast product (O'Reilly et al. 2016). Had this product been available, we could have used it to analyze biotic responses to wave energy at our sites and we might not have needed field measurements from wave sensors. However, validation along the mainland coast in the Santa Barbara Channel using two Datawell Directional Waveriders underestimated fit for energy, and had a poor fit for direction at one site. Furthermore, the CDIP model had not been validated in the Channel Islands. Given that the Channel Islands are a place with locally complex or rocky shallow water bathymetry and high degrees of sheltering (O'Reilly et al. 2016), we decided to use the WHPS sensor data to assess CDIP-hindcast accuracy.

6.2 Methods

Using our estimates for location, depth, and the normal angle of the coastline, CDIP engineers generated hourly hindcasts for height and period for each site back as far as possible using MOP v1.1 (http://cdip.ucsd.edu/MOP_v1.1/). Sites were hindcast with the same parameterization that is used for modeling the mainland coast, because that was the amount of time and effort CDIP could invest. As such, buoys were used to model island coastal waves due to their raw proximity without regard for realistic applicability. For example, the buoys in the channel were used to model seas on the south coasts of the northern islands, which may explain why they underestimate H_s there. The time range for these hindcasts began in 2000 and included dates while our sensors were deployed. Before comparing our sensor data with the CDIP hindcasts, we needed to have identically formatted data sets from the sensor (i.e., WHPS) and the hourly CDIP hindcasts calculated at grid locations near each sensor. Because of the possibility of time offsets between the sensor and CDIP wave data there could be a need for a +/- 2hr adjustment to align the benchmark and CDIP wave energies. Therefore, before analysis, we used the CDIP WaveEvalTool (<http://cdip.ucsd.edu/themes/cdip?d2=p6>) to put the sensor data into identical frequency bands and time scales as the CDIP data.

6.3 Results and Discussion

Overall, the CDIP hindcast did well at predicting site-specific wave heights and periods. Plotting CDIP model height estimates vs sensor observations (Figure 6.1) showed that, for daily averages, the CDIP model underestimated wave height across the sites. This is consistent with previous validation attempts, and is partly due to the lack of local windswell energy in the model (O'Reilly et al. 2016). Hindcast wave period tended to be less accurate, but unbiased, on average (Figure 6.2). Periods are difficult to capture in this area with a single parameter because they are often bimodal due to a mix of ground swell with local wind swell (O'Reilly et al. 2016). In the next section, we used statistical fitting to correct hindcasts for each of the monitoring sites where we put sensors, as well as for any site in the Channel Islands.

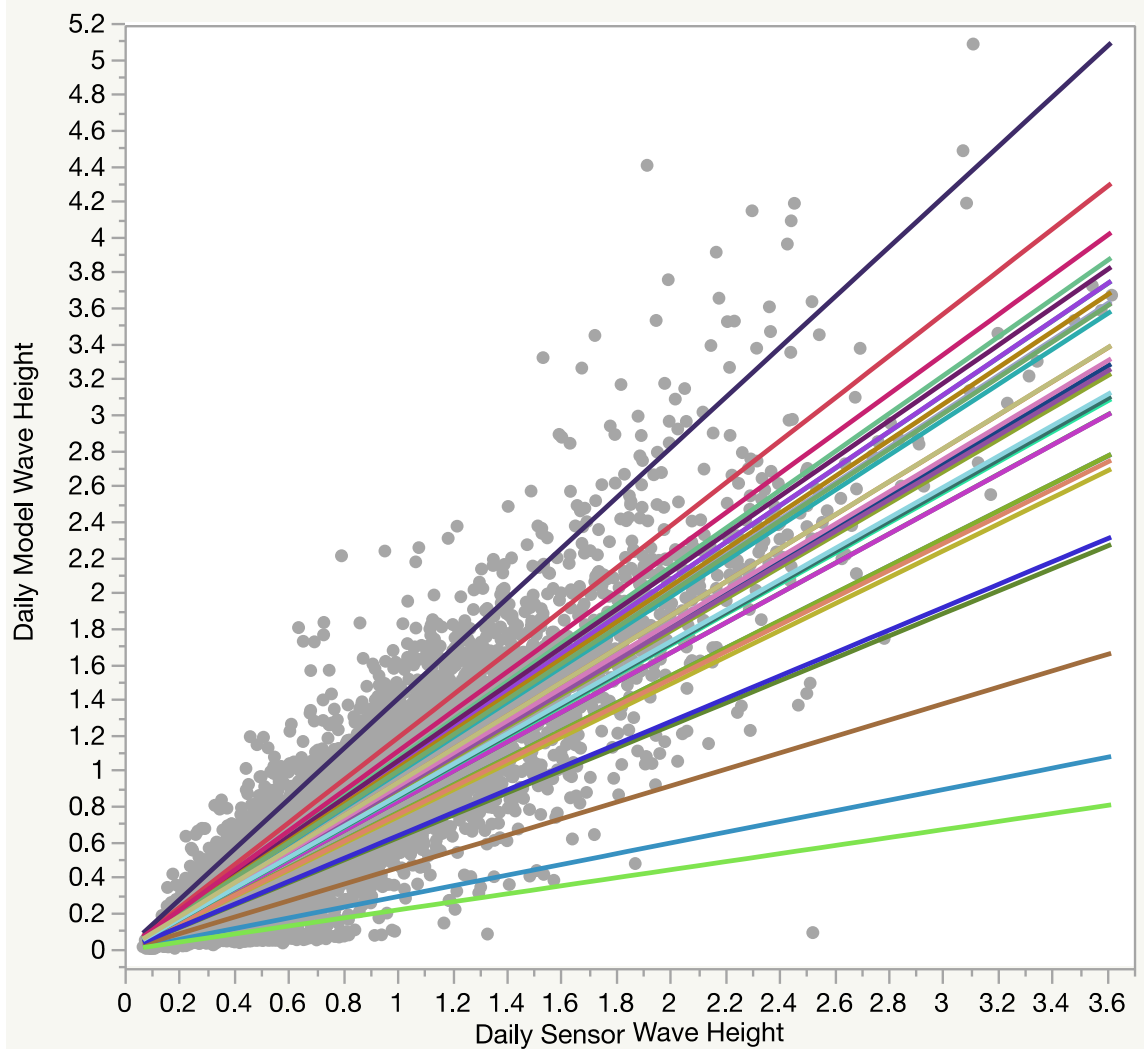


Figure 6.1. Plot of observed vs modeled daily wave height across 32 sites, with best-fit lines per site. At most, but not all sites, CDIP slightly underestimates wave height.

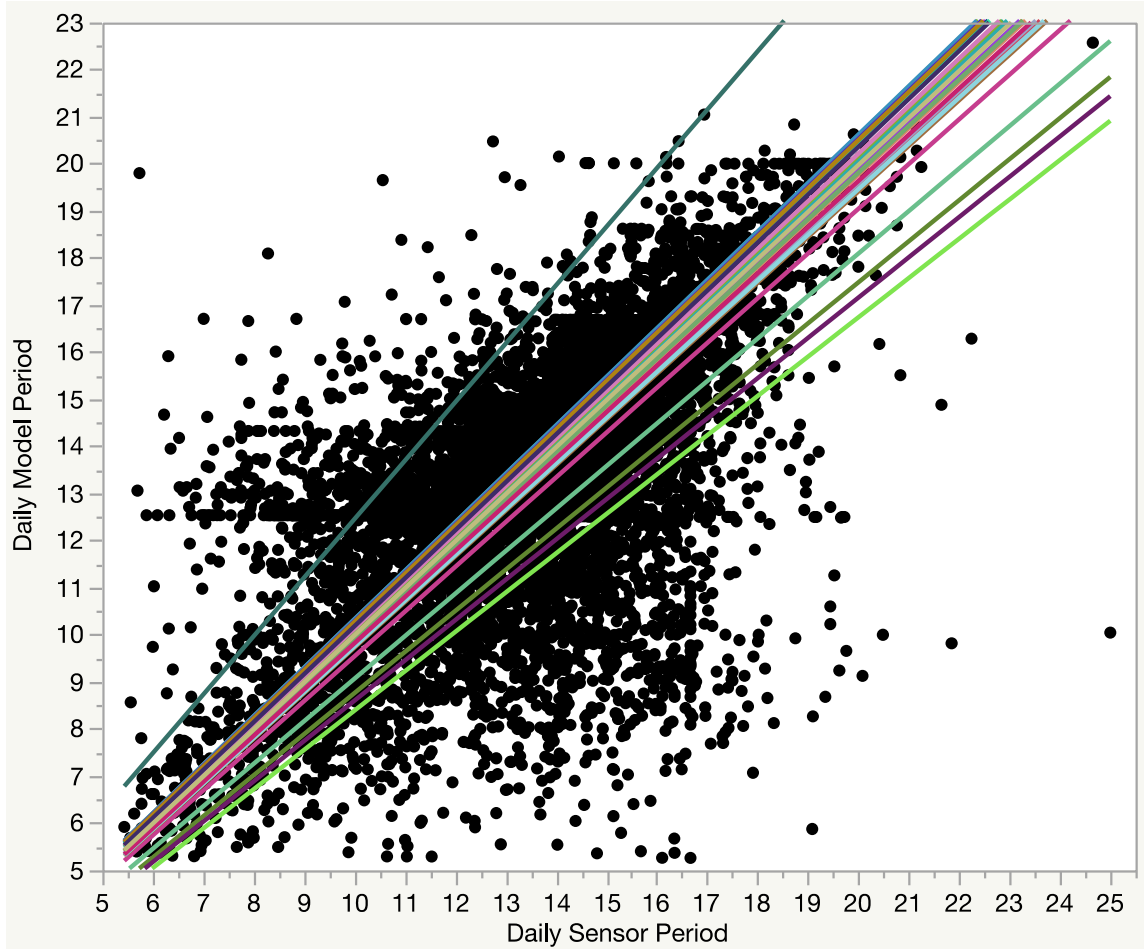


Figure 6.2. Plot of observed (Daily Sensor Period) vs modeled (Daily Model Period) daily wave period across 32 sites, with best-fit lines per site. At most, but not all sites, CDIP estimated period without bias.

7 Using Sensor Data to Correct Hindcast Bias

7.1 Introduction

We sought a simple, yet precise, statistical model to correct for the height bias described in Section 6. Doing so would allow us to correct hindcasts for the monitoring sites in our study. Because we wanted to be able to predict this correction for other sites outside our study, we sought a single coefficient correction.

7.2 Methods

Although many fitting approaches are possible, the simplest correction would be a single coefficient, which can be found using regression analysis with a zero intercept. This coefficient can be broken down into two parts, a system-wide component and a site-specific component, which sum together into a single proportional correction factor. To get this correction factor, we fit the following regression to the data: $H_s = H_m + H_m * \text{site}$, where H_s is the average daily height measured by the sensor, H_m is the daily average height from the CDIP model, and site is a categorical variable representing each sensor location. In other words, we sought to define the overall bias, and site specific biases, so that height and period CDIP estimates could be easily corrected.

7.3 Results and Discussion

The regression model for height explained 91% of the variance in the model predictions, and suggested that to correct for the tendency to underestimate wave height, CDIP height (H_m) should be multiplied by an overall bias correction of 1.18 (the average regional bias), +/- a site-specific bias coefficient (Table 7.1).

Although this simple approach worked surprisingly well, precision was lacking for two sites, PRF and RRX. PRF (Pedro Reef) is a protected site on Santa Cruz Island with small wind waves under most conditions. The three sensors deployments were consistent and seemed free from errors. However, CDIP consistently underestimated wave height, especially for south-east swells which wrap around the eastern tip of Santa Cruz Island. Adding an intercept and the swell angle A_b from Harvest Buoy (NDBC46218), removed the bias and improved the precision from $R^2 = .04$ to $R^2 = .38$. Model: $H_s = 1.17 + .062 H_m - 0.003 A$. RRX (Rodes Reef) is an exposed site on the north shore of Santa Rosa Island. The CDIP model underestimated wave height for most directions at RRX. H_s was better fit directly with Harvest height H_b , Harvest period T_b , and Harvest direction A_b . This improved the precision fit from $R^2 = .08$ to $R^2 = .57$. The regression model for RRX is $H_s = .32 H_b - .026 T_b + .002 A_b - .001 (T_b - 12.6) (A_b - 280)$.

We then asked whether there were site characteristics that could help explain the site to site variation in the correction coefficients. If so, we could improve CDIP model hindcasts at sites without sensor data. We first transformed the coefficient using the natural log to give equal weight to over and underestimates. We found that CDIP underestimated wave heights at sites with narrow swell windows (W in degrees), especially in the Northern Channel Islands. In addition, CDIP tended to underestimate height at south-facing coastlines in the Northern Channel Islands and overestimate height at north-facing coastlines in the Southern Channel Islands (Where L is latitude in decimal degrees, and +/- is positive for south facing coastlines and negative for north facing coastlines). This is not surprising because the hindcast model used channel buoys (north of the islands) to model open ocean seas south of the islands. The regression (no intercept): $\text{Ln}[\text{Coefficient}] = .018 L - .005 W - .017 (L - 33.8)(W - 102) +/- (.22 + .98(L - 33.8))$ has a precision of $R^2 = .56$ and can be used to correct these MOP hindcasts in the Channel islands, given a

measured swell window and location. Specifically, the wave height at a site that is not ground-truthed can be estimated as $H = H_m * \text{Exp}[\.0181 L - .005 W - .0168 (L - 33.8)(W - 102.4) +/- (.219 + .977(L - 33.8))]$. As an example, for a north-facing site like Scorpion Anchorage on Santa Cruz Island: $L = 34.04776$ and $W = 4$ the indirectly estimated bias coefficient would be $\text{Exp}[0.54] = 1.72$ (compared to the directly computed bias coefficient for this site of 1.58).

We applied a similar approach to correcting wave period. We fit $T_s = T_m + T_m * \text{site}$. This model explained 57% of the variance in the model predictions, and suggested CDIP hindcast period should be multiplied by 1.01, +/- a site-specific additive bias coefficient (Table 7.2).

Although bias was small for most sites, precision was relatively low, and nearly lacking for five sites, CCX, LCX, PBX, PRF and RRX. CCX (Cathedral Cove) is a sheltered site on the north coast of East Anacapa Island. This site was well predicted by the dominant period from Harvest Buoy (NDBC46218), $T_s = 4.7 + 0.52 T_b$. This improved fit from $R^2 = .13$ to $R^2 = .46$. LCX (Landing Cove) is another sheltered site on the north coast of East Anacapa Island. Because CDIP underestimated south swell periods at this site, period was better predicted by including swell direction from Harvest Buoy (NDBC46218), $T_s = 7.7 + 0.59 T_m - .006 A$. This improved fit from $R^2 = .21$ to $R^2 = .32$. PBX (Pelican Bay) is a sheltered site on the north coast of Santa Cruz Island. Because CDIP underestimated south swell periods at this site, period was better predicted by including swell direction from Harvest Buoy (NDBC46218), $T_s = 5.7 + 0.58 T_m$. This improved fit from $R^2 = .25$ to $R^2 = .57$. PRF (Pedro Reef) is a protected site with small wind waves under most conditions. CDIP underestimated wave period, especially for smaller swells. Adding an intercept and the wave height and season improved the precision from $R^2 = .08$ to $R^2 = .24$. Model: $T_s = 6.7 + 0.54 T_m + .27 H_m + 2.4(T_m - 12.1)(H_m - 0.1) +/- .44$, where +/- is positive for summer and negative for winter). As noted before, RRX (Rodes Reef), is an exposed site on the north shore of Santa Rosa Island. Here, the CDIP model overestimated wave period for small wave heights. Just as for height, period at the sensor T_s was better fit directly with buoy period T_b from platform Harvest. This improved the precision fit from $R^2 = .17$ to $R^2 = .52$. $T_s = .30 + .81 T_b$. There are some gaps in the Harvest Buoy record. We filled these gaps using the correlated hind casts from all other sites using Multivariate SVD Imputation (and setting any negative values to 0) from the JMP Pro 13.0™ platform.

As we did for height, we looked to see if we could improve CDIP period hindcasts at sites without sensor data. Ideally, one would be able to use the MOP model to generate hindcasts for the south side of the islands based on appropriate buoys. In lieu of that, however, we first transformed the bias coefficient using the natural log to give equal weight to over and underestimates. CDIP underestimated wave period at sites with narrow swell windows (W in degrees). In addition, CDIP tended to underestimate period at south-facing coastlines (where +/- is positive for south facing coastlines and negative for north facing coastlines). CDIP also underestimated period at sites with a northern swell window (C in degrees), especially in the south (where L is latitude in decimal degrees). The regression: $\text{Ln}[\text{Coefficient}] = -0.0055 L - .00154 W + .00149 C + -0.0019 (C - 224) (L - 33.8) +/- .16$ has a precision of $R^2 = .46$ and can be used to improve CDIP period hindcasts in the Channel Islands given a measured swell window (center and width) and location. Specifically, the wave period at a site that is not ground-truthed can be estimated as $T = T_m * \text{Exp}[-0.0055 L - .00154 W + .00149 C + -0.0019 (C - 224) (L - 33.8) +/- .16]$. As an example, for a north-facing site like Scorpion Anchorage on Santa Cruz Island: $L = 34.04776$, $W = 4$, and $C = 296$, the indirectly estimated bias coefficient would be $\text{Exp}[0.052] = 1.05$ (compared to the directly computed bias coefficient for this site of .99, which, ironically, would slightly reduce accuracy at this site). Given that others might want to apply corrections to other sites of interest, we curated and published the correction coefficients and equations (Lafferty and Morton 2018).

Table 7.1. List of total (1.18 + site) per-site bias (standard error), total correction coefficient (inverse of total bias), and R² for a simple no-slope model for wave height. Multiplying H_m by the correction coefficient gives the corrected wave height for a site. * indicates where CDIP hindcast was such a poor fit to the sensor that regressions based on archived Harvest Buoy (NDBC46218) data were used in addition to or instead of the CDIP hindcasts (see below).

Site	Bias	Std Error	Coefficient	R ²
APX	1.17	0.006	0.85	0.60
ARX	0.63	0.004	1.57	0.86
CAT	0.76	0.002	1.32	0.89
CCX	0.90	0.008	1.11	0.43
CPX	0.97	0.001	1.03	0.93
CSA	1.03	0.002	0.97	0.83
CVP	0.71	0.002	1.42	0.76
DTN	0.97	0.002	1.03	0.94
EDH	0.82	0.002	1.21	0.92
EFC	0.76	0.004	1.32	0.9
FHX	0.29	0.005	3.42	0.87
GCX	0.99	0.002	1.01	0.88
GIX	0.89	0.003	1.12	0.82
HRX	1.01	0.002	0.99	0.89
JLN	0.95	0.003	1.06	0.71
JLS	0.91	0.002	1.10	0.82
KHX	0.73	0.006	1.37	0.44
LCX	0.63	0.003	1.58	0.58
LHX	0.88	0.003	1.14	0.83
MMX	0.99	0.002	1.01	0.87
NFX	1.04	0.002	0.97	0.90
PBX	0.46	0.007	2.19	0.83
PRF*	0.23	0.004	4.26	0.04
RRX*	0.85	0.003	1.18	0.08
SAX	0.63	0.003	1.58	0.82
SER	0.91	0.002	1.10	0.92
SES	0.99	0.003	1.01	0.75
SPX	1.02	0.002	0.98	0.76
WAX	0.84	0.001	1.19	0.82
WEX	1.40	0.002	0.71	0.87
WLX	1.12	0.002	0.89	0.85
YBX	0.86	0.003	1.17	0.87

Table 7.2. List of bias (standard error), correction coefficients (inverse of bias), and R² for a simple no-slope model for wave period. List of bias (standard error), correction coefficients (inverse of bias), and R² for a simple no-slope model. Multiplying the CDIP hind cast by the coefficient gives the corrected wave period for a site. * indicates where CDIP hindcast was such a poor fit to the sensor that regressions based on the Harvest Buoy data were used (see below).

Site	Bias	Std Error	Coefficient	R ²
APX	0.96	0.010	1.05	.51
ARX	0.97	0.017	1.03	.51
CAT	1.00	0.006	1.00	.70
CCX*	0.94	0.009	1.06	.13
CPX	0.99	0.007	1.01	.69
CSA	0.98	0.005	1.02	.56
CVP	1.01	0.006	0.99	.78
DTN	0.99	0.006	1.01	.81
EDH	1.01	0.006	0.99	.72
EFC	1.00	0.009	1.00	.72
FHX	1.00	0.009	1.00	.27
GCX	0.94	0.006	1.06	.64
GIX	0.97	0.005	1.03	.60
HRX	0.90	0.005	1.12	.46
JLN	1.01	0.005	0.99	.67
JLS	1.01	0.004	0.99	.65
KHX	0.94	0.007	1.06	.35
LCX*	0.84	0.005	1.19	.21
LHX	1.01	0.005	0.99	.69
MMX	0.97	0.005	1.03	.54
NFX	0.83	0.007	1.21	.55
PBX*	0.96	0.005	1.04	.25
PRF*	0.80	0.005	1.25	.08
RRX*	1.18	0.009	0.85	.17
SAX	1.01	0.005	0.99	.27
SER	1.00	0.005	1.00	.73
SES	1.00	0.008	1.00	.84
SPX	0.97	0.004	1.03	.47
WAX	0.91	0.007	1.10	.74
WEX	0.99	0.007	1.01	.74
WLX	0.97	0.006	1.03	.41
YBX	0.97	0.001	1.03	.57

8 Building a Corrected Hindcast Database for Wave Energy at Kelp Forest Monitoring Sites

8.1 Introduction

Before we could implement our goal to relate biotic responses to wave energy, we needed to correct hindcasts for all our sites. We also wanted to create a wave-energy database that others could use to explore relationships between wave energy and kelp-forest communities.

8.2 Methods

Using the bias correction coefficients in Section 7, and the statistical models for sites not well fit by the bias correction, and the derived statistical models for sites without past sensor data, we generated site-specific hourly wave hind casts from 2000 through 2017.

In addition, we were assisting with a larger effort to merge several databases for the study region, meaning that we could use Lafferty and Morton (2018) to expand our site list for an additional 56 sites, bringing our total sites to 88. However, given the annual nature of the biological data, these wave data were summarized annually (for the 12 month interval and 6 month interval before biological data collection for a particular site-year combination).

8.3 Results and Discussion

The hindcast database includes 383,942 site-specific hourly wave hind casts with the following data columns: year_utc, month_utc, day_utc, hour_utc, cdip_Hs_m, cdip_Tp_sec, cdip_Dp_degTrue, adjusted_cdip_Hs_m, mean_sensor_pressure_dbar, Transect_depth_m, ubr_Sensor, Tbr_sensor, wave_energy, date, juliand, season, wyr, waveyr, season_yr, Hs_corrected, Tp_corrected, ubr_corrected, Tbr_corrected, wave_energy_corrected. The full dataset has been curated, published, and made available as Lafferty et al. (2018). We used a similar study as an example for how to calculate and use “wave energy” (Williams et al. 2013). Bottom orbital velocity was calculated after Wiberg and Sherwood (2008).

The larger 88-site database includes wave data on mean height, energy, and orbital velocity calculated at 6- and 12-month intervals before biotic sampling. The wave data in Lafferty et al. (2018) were integrated into a large integrated data table produced by the Santa Barbara Channel Marine Biodiversity Observing Network (<http://sbc.marinebon.org/>) available at the following DOIs:

doi:10.6073/pasta/1345f0148e6dfe4df9065e223b4dd783

doi:10.6073/pasta/bf143fa962e1edb822847bc0ee90c2f7

doi:10.6073/pasta/51d2db26e90d4b8687db81fb40bc58c4

doi:10.6073/pasta/d09d4bfd54e6d4e490b4cc34731d808e

9 Estimating Biological Responses to Wave Energy

9.1 Introduction

Kelp forests are impacted by wave exposure, yet adapted to average conditions in the region (Bell et al. 2015). Wave action has positive and negative features for organisms. It creates hydrodynamic stressors that can dislodge individuals, and it also provides flow that can transport materials such as nutrients and food (Shields et al. 2011). These contrasting effects could influence various ecological factors, such as recovery rates from disturbance, productivity and biodiversity. Furthermore, given the various food-web interactions in marine systems, indirect effects of waves are also possible. For instance, one way that waves likely affect species is in how they affect that species' prey, predators and parasites (Shields et al. 2011).

Examining how species respond to wave exposure requires community time series data on ecological communities from several different sites. Such a long-term data set was organized and analyzed by the BOEM-funded *DOI Partnership: Distinguishing Between Human and Natural Causes of Changes in Kelp Forests Using Long-term Data from DOI Monitoring Programs*. These data are taken annually, meaning that we first needed to match annual wave energy measures from Lafferty and Morton (2018). A subset of these wave data are now incorporated into the integrated data set, making it possible to create statistical models that express nearshore communities as a function of wave energy in time and space. With such statistical models, it should be possible to estimate a change in community state that might result from a change in wave energy state data derived from the *DOI Partnership* study. From these data, we asked how organismal density responds to wave energy.

Other researchers have asked similar questions, albeit for different reasons. For instance, sea grass meadows cannot persist under high wave energy, which might increase under sea level rise. By modeling the association of sea grass to a wave-energy gradient, Saunders et al. (2014) was able to predict 10-85% reductions in sea grass cover in shallow habitats after a 1m sea level rise (and no reef accretion). European kelps vary in their response to wave energy (Gorman et al. 2012), suggesting that species-specific responses to wave energy could also vary in our region.

9.2 Methods

As part of the BOEM-funded *DOI Partnership* study, we incorporated our wave data into a broader data set assembled by the Santa Barbara Channel Marine Biodiversity Observation Network, which contains information about the densities of algal, invertebrate, and fish taxa, as well as environmental covariates. In our analyses, the dependent variable was organismal abundance for a particular taxon. Organismal abundance was averaged over all replicate transects for each site-date combination, subject to three constraints. For each taxon, we excluded sites combinations where the taxon was reported at < 20% of sampling dates (because we assumed habitat conditions were poor, or out of range, for this particular taxon at this particular site). To minimize seasonal effects, we excluded observations taken outside the June-October sampling window (this has the advantage of standardizing, with the disadvantage of missing observations from Santa Barbara Island and Anacapa Island). After imposing these restrictions, we further excluded rare taxa, as those with < 100 observations. To help meet assumptions of the general linear model, we transformed organismal density with the square root prior to statistical analysis.

The wave variables were bottom orbital velocity (m/s) calculated over the 12 months before the date each ecological observation was collected. We chose orbital velocity because this was likely most related to the

physical experience of the benthic organisms tracked in the biological data. Furthermore bottom orbital velocity is a non-linear function of wave energy and depth (Wiberg and Sherwood 2008). By including bottom orbital velocity and depth in our analysis, we could consider the independent effects that depth might have apart from attenuating wave energy (e.g., reducing light, or increasing nutrients). Each wave measure was taken from corrected hourly wave heights, periods and depths (as described previously). Given the possibility that wave energy had a non-linear effect on taxon density, we also included bottom orbital velocity squared as potential predictors.

The fixed effect covariates used were 12-month mean sea surface temperature (and its square), Log transformed 12-month mean Chlorophyll (within a 3 km buffer), Log transformed 12-month mean diffuse attenuation (a measure of water turbidity), % sand, Depth (m), and the categorical variables: fished/unfished, island/mainland. Site and year were treated as random effects and representing site-specific habitat characteristics or annual variation not explained by the other covariates.

We report the model coefficients (and their standard errors) in two ways: all variables included, or all non-significant variables excluded (the pruned model), the latter being an attempt to both reduce over fitting and increase power. When removing variables with squared terms, we always removed the squared term before removing the linear term. For our questions, results were consistent between each approach.

To estimate taxon sensitivity to wave energy we simply report the pruned model coefficients for bottom orbital velocity (after controlling for other factors), with an emphasis on the significance and magnitude of the density response.

9.3 Results and Discussion

Across all species, only 12% of the variation in abundance in time and space was explainable by the fixed covariates in our study. Unmeasured site characteristics (e.g., habitat complexity) explained 32% of the variation on average (algae = 50%, invertebrate = 51%, fish = 20%), and unmeasured annual characteristics (e.g., a strong recruitment year or disease outbreak) explained 11% (algae = 4%, invertebrate = 9%, fish = 13%). That left an average of 45% of the variation unexplained. Unexplained variance could be due to measurement error, intra-annual variation, seasonality, or species interactions.

Each covariate explained some variance in the density of at least one species (Table 9.1). By far, sea surface temperature explained the most variance, followed by wave orbital velocity, island/mainland, chlorophyll, diffuse attenuation, and fishing. Species sensitivity to orbital velocity varied across taxa. For 36 of the 56 taxa, density was not statistically associated with orbital velocity (Table 9.1).

Table 9.1. Significant standardized regression coefficients indicating density associations by species (algae in green, invertebrates in red and fishes in blue text), to various potential drivers. Colored shading in a cell corresponds to coefficient magnitude and sign (with dark red being strongly negative and dark blue being strongly positive). SST = 12-month average sea surface temperature, OV = 12-month mean bottom orbital velocity, island = island/mainland, depth = transect depth in m, Chl. = satellite derived 12-month average log chlorophyll concentration within a 3 km buffer, sand = % sand on transect, DA= satellite derived 12-month average diffusion attenuation, fish = fishing/reserve.

Species	SST	SST ²	OV	OV ²	island	depth	Chl.	sand	DA	fish
<i>Egrecia menziesii</i>						-0.38				
<i>Eisenia arborea</i>										
<i>Laminaria farlowii</i>							-0.45			
<i>Macrocystis pyrifera</i> biomass	-0.24		0.81	-0.52						
<i>Macrocystis pyrifera</i> density	-0.50	0.48								
<i>Pterygophora californica</i>	-0.36								0.16	
<i>Aplysia californica</i>	2.06	-1.85			0.30					
<i>Apostichopus parvimensis</i>	-0.05		-0.14		0.34	-0.24				-0.44
<i>Crassadoma gigantea</i>	0.28				0.31					
<i>Kelletia kelletii</i>					-0.46	0.29				
<i>Megastraea undosa</i>	0.44				0.19					
<i>Megathura crenulata</i>	-0.12									
<i>Mesocentrotus franciscanus</i>	3.14	-3.15			0.40			-0.23		
<i>Neobernaya spadicea</i>						0.27	-0.17	-0.21		
<i>Patiria miniata</i>	-0.31				0.25	0.45				
<i>Pisaster giganteus</i>	-0.59		-0.47	0.37					0.15	
<i>Pycnopodia helianthoides</i>	-3.75	3.19			0.23					
<i>Stephanocystis osmundacea</i>	0.15									
<i>Strongylocentrotus purpuratus</i>	5.55	-5.41			0.33	-0.21		-0.15		
<i>Styela montereyensis</i>	-0.19									
<i>Tethya aurantium</i>						0.50	0.30			
<i>Urticina lofotensis</i>								-0.15		
<i>Aulorhynchus flavidus</i>	-0.33									
<i>Brachyistius frenatus</i>					-0.10					
<i>Caulolatilus princeps</i>	-5.41	5.67	-0.18						0.14	

Species	SST	SST ²	OV	OV ²	island	depth	Chl.	sand	DA	fish
<i>Chromis punctipinnis</i>	0.34	0.19	-0.66	0.51	0.22					
<i>Cymatogaster aggregata</i>			-0.18							
<i>Embiotoca jacksoni</i>			-1.01	-1.01	-0.36					
<i>Embiotoca lateralis</i>	-0.20		0.35		0.36					
<i>Girella nigricans</i>			-1.21	0.90		-0.14				
<i>Gymnothorax mordax</i>	0.31									
<i>Halichoeres semicinctus</i>	-5.67	6.25	-0.29			-0.10				
<i>Heterodontus francisci</i>	-0.02									
<i>Hypsurus caryi</i>	2.64	-2.80				0.24	0.15			
<i>Hypsypops rubicundus</i>	-1.21	1.43	-1.45	1.12	0.18	-0.28				
<i>Medialuna californiensis</i>	-3.98	4.28	-0.68	0.42						
<i>Myliobatis californica</i>						-0.11			0.17	
<i>Ophiodon elongatus</i>	4.07	-4.23								-0.32
<i>Oxyjulis californica</i>	0.24									
<i>Paralabrax clathratus</i>	-2.32	2.73	-1.03	0.74	-0.19	-0.13				
<i>Phanerodon furcatus</i>	-0.21							0.41	0.24	
<i>Rhacochilus toxotes</i>			-0.54	0.39	-0.22		0.13			
<i>Rhacochilus vacca</i>			-0.72	0.53			0.35			
<i>Scorpaenichthys marmoratus</i>						-0.19	0.24			
<i>Sebastes atrovirens</i>	-0.26									
<i>Sebastes auriculatus</i>					-0.41					0.21
<i>Sebastes carnatus</i>	-0.13		-0.68	0.61	-0.26			-0.31		
<i>Sebastes caurinus</i>	-0.23									
<i>Sebastes chrysomelas</i>	-0.63	0.45								
<i>Sebastes miniatus</i>			0.24							
<i>Sebastes mystinus</i>	3.51	-3.41	0.19		0.07	0.23				
<i>Sebastes paucispinis</i>							0.02		-0.02	
<i>Sebastes rastrelliger</i>								0.23		
<i>Sebastes serranoides</i>			0.20		0.14		0.03	0.02		
<i>Sebastes serriceps</i>	1.74	-1.74	-0.72	0.53						
<i>Semicossyphus pulcher</i>	-1.27	1.68			0.19				0.10	

Surprisingly, no macroalgal densities responded to wave energy. This is in contrast to other studies that show community level responses, with higher macroalgal diversity at intermediate wave-energy sites in Western Australia (England 2008). On the other hand, consistent with past results (Bell et al. 2015), kelp biomass (dashed line) peaked at intermediate orbital velocity (Figure 9.1).

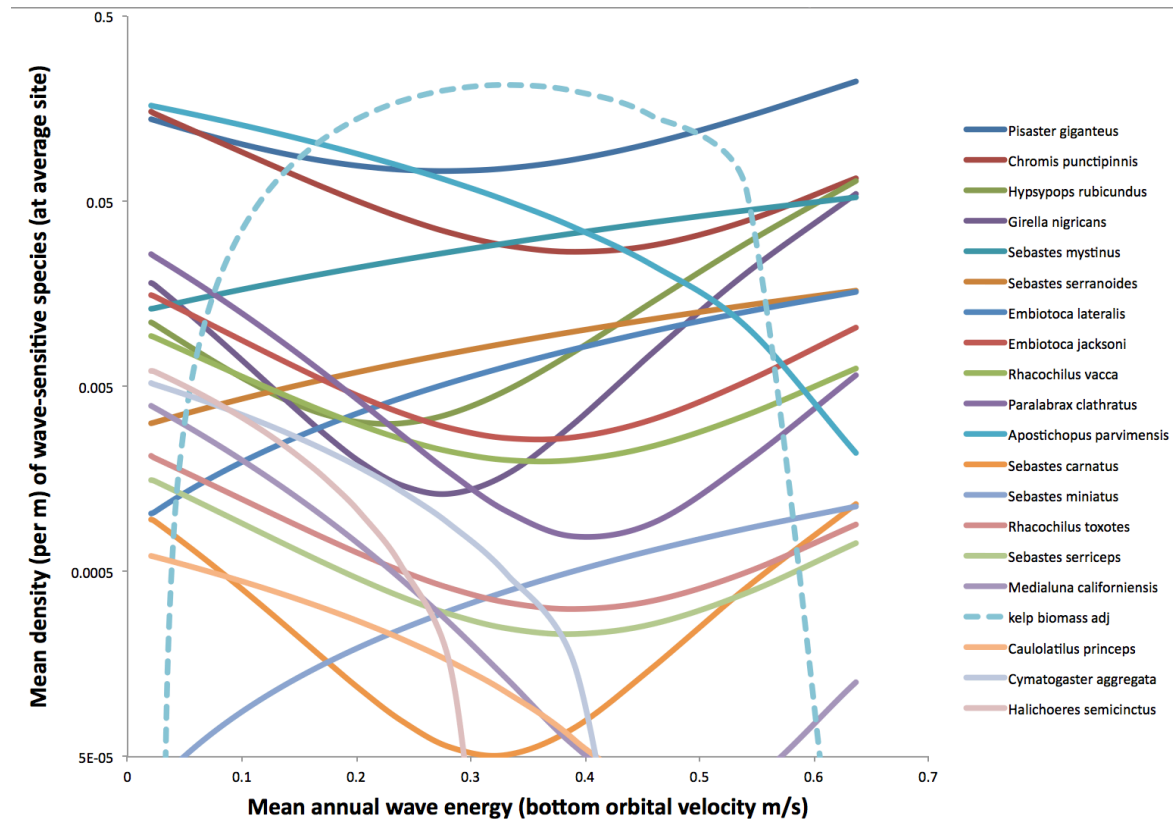


Figure 9.1. Modeled species density (note the logged axis) plotted against orbital bottom velocity for 20 species with significant responses to wave energy. Across all 395 site-year combinations, annual wave velocity ranged from 0.02 to 0.63 with a mean of 0.19 m/s. Kelp biomass adjusted (adj) is kelp biomass (kg/m^2) divided by 1,000,000 to have comparable units).

Twenty species were statistically associated with bottom orbital velocity, often in complex ways. Four species (*Apostichopus parvimensis*, *Caulolatilus princeps*, *Cymatogaster aggregata*, and *Halichoeres semicinctus*) had negative associations, whereas four species (*Sebastes mystinus*, *S. serranoides*, *Embiotoca lateralis*, *S. miniatus*) had positive associations. The remaining twelve species unexpectedly reached minimum density at medium orbital velocities. This variation among species is consistent with other studies that have found fishes have different responses to wave energy, with few species adapted to highly turbulent conditions (Munks et al. 2015). Although we can only speculate about why these species differed with respect to their association with wave energy, the species associated with calmer water included a benthic sea cucumber (*A. parvimensis*) that cannot attach firmly to the substrate, a small surf perch (*Cymatogaster aggregata*) whose distribution includes calm bays and estuaries, and a rock wrasse (*H. semicinctus*) and ocean whitefish (*Caulolatilus princeps*) that tend to associated with sandy habitat, which might be more stable in calmer areas. The rockfishes associated with higher wave energy are less easy to explain. For instance, blue rockfish (*S. mystinus*) move deeper when wave energy is high (Green

et al. 2014), and were not associated with wave energy in another study (Young and Carr 2015). Furthermore, Young and Carr (2015) found that *S. serranoides* and *Embiotica lateralis*, were more often found at sites with low wave energy, rather than, as found here, at sites with high wave energy. Furthermore, the one fish species that Young and Carr (2015) found was associated with high wave energy (*Sebastes chrysomelas*) was not associated with wave energy in our study. Such inconsistencies suggest that the effects of wave energy are either weak or masked by other drivers, though there are many other difference, such as Young and Carr (2015) using general additive models and including as explanatory variables: depth, substrate, slope, kelp biomass and orbital velocity (meaning that their response to orbital velocity was considered after accounting for the interactions with kelp, which is known to drive species distributions and be affected by wave energy).

At this point we do not have a hypothesis for what would create such a pattern, but it could be an indirect response to a parameter, like kelp biomass, that has the opposite pattern. Because the relationship with wave energy was often non-linear, it is difficult to predict the directional effect of wave energy extraction on species abundances. Notably, fish move and their counts can be highly variable, perhaps in response to recent wave events. Our statistical predictions use long-term average wave energy, yet snapshot observations could be affected by recent storms. However, most sampling occurs during calm conditions. Other non-linear approaches, such as knotted splines or additive models would be more appropriate for assessing species-level responses to wave energy not attempted here.

10 Predicting the Consequences of Wave Energy Absorption from Marine Renewable Energy Facilities on Nearshore Ecosystems

10.1 Introduction

Given that several taxa respond to wave energy, we might expect that renewable energy facilities could lead to significant changes in their density. Therefore, we sought to see how the species that were associated with wave energy responded to a 15% reduction in wave height, which is the upper end of expected wave height reduction due to renewable energy facilities (EPRI 2004, Nelson et al. 2008). Here, the general expectation is that wave energy is a disturbance that impacts giant kelp and associated species, shifting the community toward high-energy specialists (*Egregia* and surfgrass) and their associated species (Parnell 2015). For instance, intense wave energy in Central California impairs kelp canopy persistence, leading to lower overall biomass density of kelps in Central California than in Southern California, despite the higher nutrients and lower grazing pressures in Central California (Reed et al. 2011). However, non-linearities in the biological response (Figure 9.1) could result in a situation where organisms at low energy sites respond differently from organisms at high-energy sites. Here we focus on high-energy sites where renewable energy projects might occur (Shields et al. 2011).

10.2 Methods

Our approach builds on the statistical models described in Section 9. Orbital velocity is roughly proportional to wave height, so a 15% reduction in wave height will result in a 15% reduction in orbital velocity. To estimate taxon sensitivity to a change in wave height due to hydrokinetic energy extraction, we ran the statistical models to generate the best-fit predictions for taxon density. We set non-wave related parameters to their grand means (and assumed that wave energy extraction would not affect them). For the categorical variables, we chose the most common states: fished and island.

To simulate species densities at a site where wave energy extraction might occur (e.g., high energy sites), we fit the previous model of species densities to the 97.5% upper quantile for mean annual orbital velocity at a site (e.g., 0.46 m/s). We used the profiler feature in JMP Pro 13.0™ to calculate the expected mean and 95% confidence limits for species density under such high energy conditions. For the “after” model we chose a 15%-lower wave orbital velocity (i.e., $0.46 * 0.85 = 0.39$ m/s), and recalculated the predicted density and confidence limits. To focus the results on species with significant sensitivity to wave energy, this was done for pruned models only. We plotted species densities before and after a 15% reduction in wave energy to estimate if there are likely to be any statistically significant biological responses to reducing wave energy at high wave energy sites.

10.3 Results and Discussion

Density responses to a 15% reduction in wave height at an exposed site varied across species, but such a reduction never altered density significantly ($P < 0.05$) (given the existing sampling effort), as seen graphically by comparing the 95% confidence limits between the before and after bars (Fig. 10.1). This suggests that although some species do respond to the range in bottom orbital velocity seen in our study system, a 15% reduction in wave height at a high wave energy site was too subtle for the models to predict a detectable change in any species density. Figure 10.1 shows these effects for wave sensitive species only (insensitive species would have no change), listed from most abundant under high wave energy.

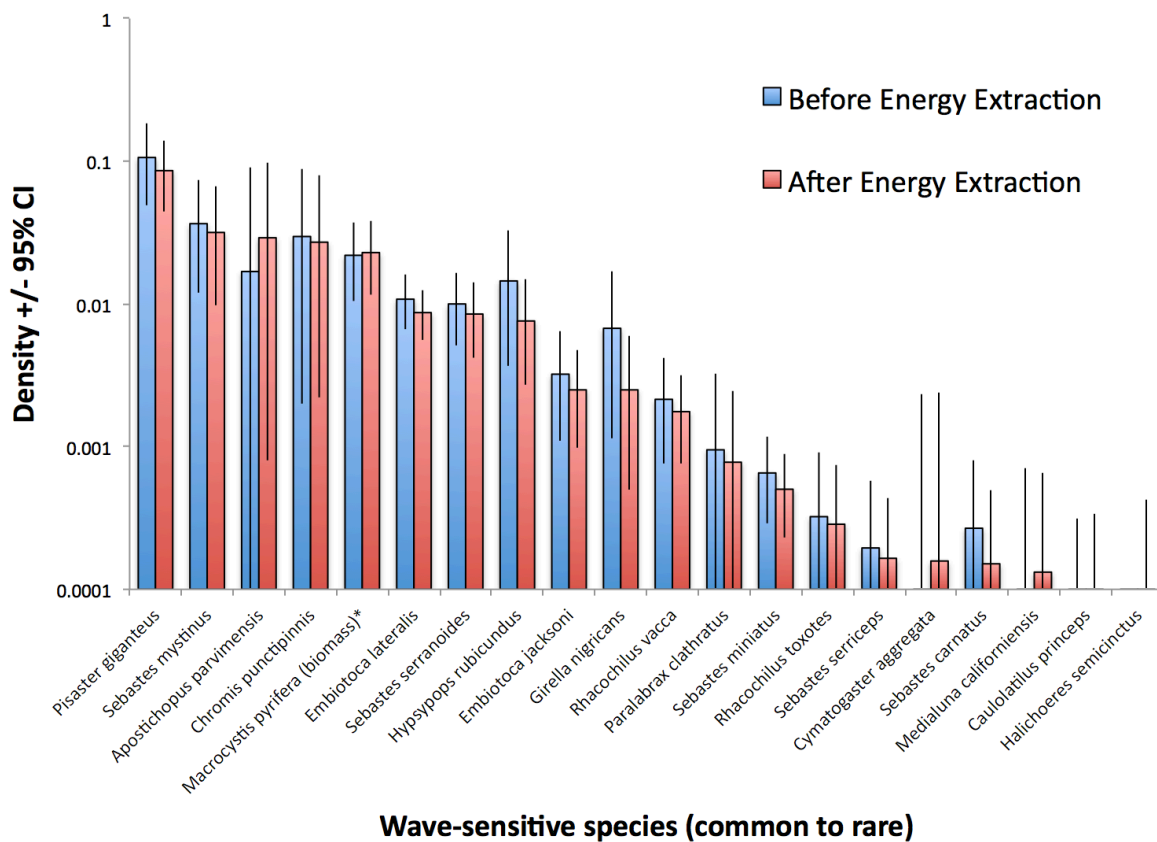


Figure 10.1. Modeled species densities before (blue) and after (red) a 15% reduction in wave height at an exposed site. Confidence limits all overlap the before-after comparison, indicating no statistically detectable change of wave energy extraction, even for the 20 species (and kelp biomass) with significant responses to wave energy. Kelp biomass is divided by 1,000,000 to have comparable units).

Although none of the modeled changes were statistically significant, some patterns in the data are worth speculating about. Firstly, although we pose our hypothesis in terms of changes in abundances, species could also respond by changing their depth distributions, further lessening the site-level effects predicted. If there was to be an effect of reducing wave energy at high-energy sites, these results suggest up to 14 of the 56 species could decline slightly as a response, whereas some species might respond positively, most notably kelp biomass and the sea cucumber *Apostichopus parvimensis*. In particular, reducing wave energy might allow two fish species (*Cymatogaster aggregata* and *Medialuna californiensis*) to persist where they could not before, but for two wave-intolerant fish species (*Caulolatilus princeps* and *Halichoeres semicinctus*), a 15% reduction in wave height would not be sufficient to allow them to persist. Effects in deeper water (or far from a wave energy extraction device) should be even more subtle (and in shallower water more substantial) than estimated. To put these results in context, Young and Carr (2015) similarly predicted that kelp forest fish species richness declines with wave orbital velocity, suggesting that, if anything reducing wave energy by 15% would increase fish diversity in kelp forests. These results can inform the streamlining of predictions for the effects of renewable energy projects on temperate kelp forest communities and be used as a guide when planning associated monitoring.

11 References

- Bell, T.W., Cavanaugh, K.C., Reed, D.C. and Siegel, D.A., 2015. Geographical variability in the controls of giant kelp biomass dynamics. *Journal of Biogeography*, 42(10), pp.2010-2021.
- Boehlert, G., Braby, C., Bull, A.S., Helix, M.E., Henkel, S., Klarin, P. and Schroeder, D. eds. 2013. Oregon Marine Renewable Energy Environmental Science Conference Proceedings. U.S. Department of the Interior, Bureau of Ocean Energy Management, Cooperative Agreement with Oregon State University M12AC00012. OCS Report BOEM 2013-0113. 134 pp.
- Elwany, M.H.S., O'Reilly, W.C., Guza, R.T. and Flick, R.E., 1995. Effects of Southern California kelp beds on waves. *Journal of Waterway, Port, Coastal, and Ocean Engineering*, 121(2), pp.143-150.
- England, P.R., Phillips, J., Waring, J.R., Symonds, G. and Babcock, R., 2008. Modelling wave-induced disturbance in highly biodiverse marine macroalgal communities: support for the intermediate disturbance hypothesis. *Marine and Freshwater Research*, 59(6), pp.515-520.
- EPRI. 2004. Offshore Wave Power in the US: Environmental Issues. Electric Power Research Institute report E21 Global EPRI - 007 - US, 21 December 2004.
- Erikson, L.H., Storlazzi, C.D. and Golden, N.E., 2014, Modeling Wave and Seabed Energetics on the California Continental Shelf: *U.S. Geological Survey pamphlet to accompany data release 10.5066/F7125QNQ*
- Hegermiller, C.A., Rueda, A., Erikson, L.H., Barnard, P.L., Antolinez, J.A. and Mendez, F.J., 2017. Controls of multimodal wave conditions in a complex coastal setting. *Geophysical Research Letters*, 44(24), pp.12-315.
- Hepburn, C.D., Holborow, J.D., Wing, S.R., Frew, R.D. and Hurd, C.L. 2007. Exposure to waves enhances the growth rate and nitrogen status of the giant kelp *Macrocystis pyrifera*. *Marine Ecology Progress Series*, 339, pp.99–108.
- Gaylord, B., Hale, B.B. and Denny, M.W., 2001. Consequences of transient fluid forces for compliant benthic organisms. *Journal of Experimental Biology*, 204(7), pp.1347-1360.
- Green, K.M., Greenley, A.P. and Starr, R.M., 2014. Movements of Blue rockfish (*Sebastes mystinus*) off Central California with comparisons to similar species. *PloS one*, 9(6), e98976.
- Gorman, D., Bajjouk, T., Populus, J., Vasquez, M. and Ehrhold, A., 2013. Modeling kelp forest distribution and biomass along temperate rocky coastlines. *Marine Biology*, 160(2), pp.309-325.
- Jensen, M.M. and Denny, M.W., 2015. Experimental determination of the hydrodynamic forces responsible for wave impact events. *Journal of Experimental Marine Biology and Ecology*, 469, pp.123-130.
- Lafferty, K.D., Morton, D.N., Gotschalk, C.C., Henderikx, F., Rassweiler, A. and Washburn, L., 2018, Hourly wave height and period hindcasts at 32 sites throughout the Channel Islands National Park and San Nicolas Island from 2000-2017: U.S. Geological Survey data release, <https://doi.org/10.5066/P91KH2Q7>.

- Lafferty, K.D. and Morton, D.N., 2018, Site table and bias corrections for Coastal Data Information Program (CDIP) hind casts at the California Channel Islands: U.S. Geological Survey data release, <https://doi.org/10.5066/P9FV1X7H>.
- Munks, L.S., Harvey, E.S. and Saunders, B.J., 2015. Storm-induced changes in environmental conditions are correlated with shifts in temperate reef fish abundance and diversity. *Journal of Experimental Marine Biology and Ecology*, 472, pp.77-88.
- Nelson, P.A., Behrens, D., Castle, J., Crawford, G., Gaddam, R.N., Hackett, S.C., Largier, J., Lohse, D.P., Mills, K.L., Raimondi, P.T., Robart, M., Sydeman, W.J., Thompson, S.A. and Woo, S. 2008. Developing Wave Energy In Coastal California: Potential Socio-Economic And Environmental Effects. California Energy Commission, PIER Energy-Related Environmental Research Program & California Ocean Protection Council CEC-500-2008-083.
- O'Reilly, W.C., Olfe, C.B., Thomas, J., Seymour, R.J. and Guza, R.T., 2016. The California coastal wave monitoring and prediction system. *Coastal Engineering*, 116, pp.118-132.
- Parnell, P.E., 2015. The effects of seascape pattern on algal patch structure, sea urchin barrens, and ecological processes. *Journal of Experimental Marine Biology and Ecology*, 465, pp.64-76.
- Reed, D.C., Rassweiler, A., Carr, M.H., Cavanaugh, K.C., Malone, D.P. and Siegel, D.A., 2011. Wave disturbance overwhelms top-down and bottom-up control of primary production in California kelp forests. *Ecology*, 92(11), pp.2108-2116.
- Ricketts, E.F. and Calvin, J. 1939 *Between Pacific Tides: An Account of the Habits and Habitats of Some Five Hundred of the Common, Conspicuous Seashore Invertebrates of the Pacific Coast Between Sitka, Alaska, and Northern Mexico*. Stanford University Press.
- Saunders, M.I., Leon, J.X., Callaghan, D.P., Roelfsema, C.M., Hamylton, S., Brown, C.J., Baldock, T., Golshani, A., Phinn, S.R., Lovelock, C.E. and Hoegh-Guldberg, O., 2014. Interdependency of tropical marine ecosystems in response to climate change. *Nature Climate Change*, 4(8), p.724.
- Shields, M.A., Woolf, D.K., Grist, E.P., Kerr, S.A., Jackson, A.C., Harris, R.E., Bell, M.C., Beharie, R., Want, A., Osalusi, E. and Gibb, S.W., 2011. Marine renewable energy: The ecological implications of altering the hydrodynamics of the marine environment. *Ocean & Coastal Management*, 54(1), pp.2-9.
- Wiberg, P.L., and Sherwood, C.R., 2008. Calculating wave-generated bottom orbital velocities from surface-wave parameters. *Computers & Geosciences*, 34(10), 1243-1262.
- Williams, G.J., Smith, J.E., Conklin, E.J., Gove, J.M., Sala, E. and Sandin, S.A., 2013. Benthic communities at two remote Pacific coral reefs: effects of reef habitat, depth, and wave energy gradients on spatial patterns. *PeerJ*, 1, p.e81.
- Washburn, L., Gotschalk, C.C., Rassweiler, A., Morton, D.N. and Lafferty, K.D., 2018. Hourly wave-height observations from 2013 to 2017 at 32 sites throughout the Channel Islands National Park and San Nicolas Island: U.S. Geological Survey data release, <https://doi.org/10.5066/P90QS9WZ>.
- Young, M. and Carr, M.H., 2015. Application of species distribution models to explain and predict the distribution, abundance and assemblage structure of nearshore temperate reef fishes. *Diversity and Distributions*, 21(12), pp.1428-1440.



Department of the Interior (DOI)

The Department of the Interior protects and manages the Nation's natural resources and cultural heritage; provides scientific and other information about those resources; and honors the Nation's trust responsibilities or special commitments to American Indians, Alaska Natives, and affiliated island communities.



Bureau of Ocean Energy Management (BOEM)

The mission of the Bureau of Ocean Energy Management is to manage development of U.S. Outer Continental Shelf energy and mineral resources in an environmentally and economically responsible way.

BOEM Environmental Studies Program

The mission of the Environmental Studies Program is to provide the information needed to predict, assess, and manage impacts from offshore energy and marine mineral exploration, development, and production activities on human, marine, and coastal environments. The proposal, selection, research, review, collaboration, production, and dissemination of each of BOEM's Environmental Studies follows the DOI Code of Scientific and Scholarly Conduct, in support of a culture of scientific and professional integrity, as set out in the DOI Departmental Manual (305 DM 3).